Erbium and thulium doped planar amplifier materials

J.J. Penninkhof

Supervisors: Dr. C. Strohhöfer and Prof. Dr. A. Polman

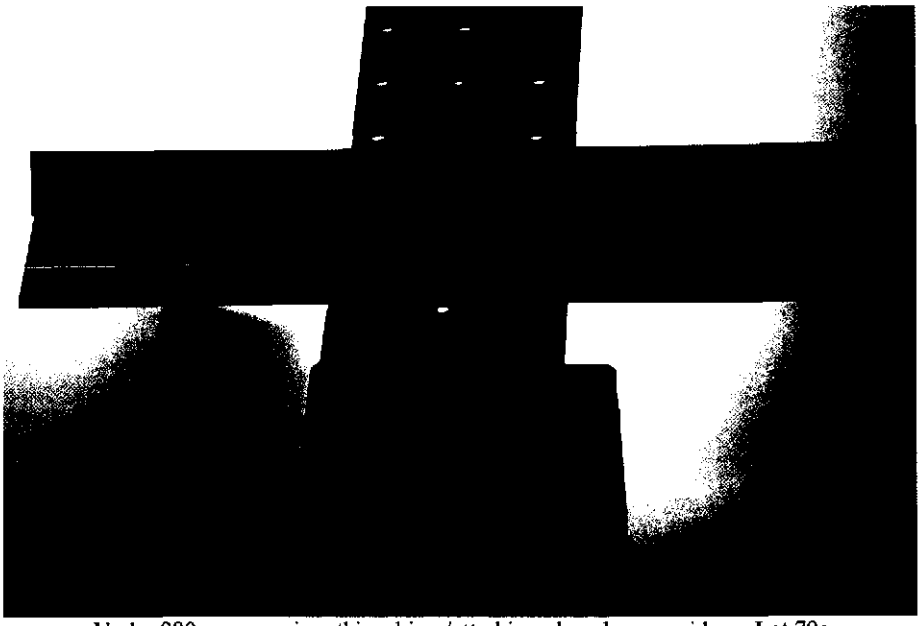

Under 980 nm pumping, this erbium/ytterbium doped waveguide on Lot 79a shows green upconversion luminescence.

Report of a research project for the masters degree in
experimental physics of Utrecht University,
performed in the period January 22, 2001 – April 1, 2002

at

AMOLF FOM

FOM-Institute for Atomic and Molecular Physics
Kruislaan 407
1098 SJ Amsterdam
The Netherlands

in collaboration with

SYMMORPHIX™

Symmorphix Inc.
1278 Reamwood Avenue
Sunnyvale CA
USA

Abstract

Optical amplification over a broad spectral range becomes more and more important since the growing use of modern communication methods. In this report the optical properties of erbium and thulium doped materials have been investigated that can be used for planar waveguide amplifiers. First, Neoceram, an Al_2O_3 / SiO_2 compound was studied. Although broad erbium luminescence was observed in the bulk material, this compound is not suitable as sputtering target since sputtered films are inhomogeneous. Samples were doped with erbium by ion implantation and the (Gaussian) depth profile is determined by RBS. We derived a simple model for ion range and straggle of erbium implantations in Neoceram and silica for energies ranging from 100 keV to 1 MeV. Furthermore, upconversion effects in two erbium/ytterbium codoped channel waveguides based on aluminasilica glass were investigated. 1.49 μm pump light was coupled into the waveguide and luminescence at 1.53 μm and 980 nm was collected from the top of the waveguide as function of pump power. The cooperative upconversion coefficient was determined at $(1.3\pm0.3)\times10^{-17}$ cm^3/s (Er concentration 7×10^{20} cm^{-3}) and $(5.5\pm0.2)\times10^{-18}$ cm^3/s (Er concentration 2.3×10^{20} cm^{-3}). For both waveguides, the excited state absorption cross section was estimated to be less than 1×10^{-21} cm^2. Under high intensity pump conditions, the decay rate due to upconversion is larger than the spontaneous emission rate of erbium.

Next, optical properties of erbium and thulium (co-)doped silica were studied. Thulium doped materials have been used to make optical amplifiers at 1.4 μm and also lasers operating at >1.7 μm have been reported. If these properties of thulium can be combined with the properties of erbium, a broadband amplifier can be made. Silica thin film samples were doped with thulium and annealed for one hour under different conditions. While erbium doped films can be annealed in vacuum to 1000 °C before precipitation sets in, thulium doped films are best annealed at 800 °C in vacuum. No luminescence in the infrared was observed after annealing at 900 °C. Excitation spectra around 800 nm were measured for singly doped silica films with erbium and thulium. By varying the pump wavelength in the region from 740 nm to 840 nm the relative excitation rate of erbium and thulium can be tuned. Under 800 nm excitation, thulium doped films show a broad luminescence spectrum extending from 1.5 μm to >1.7 μm. The luminescence lifetime at 1.6 μm is in the 100–200 μs range. In contrast, lifetimes measured at 794 nm and at 647 nm are as long as 0.20±0.02 ms and 0.21±0.03 ms respectively. In erbium/thulium co-doped silica films a characteristic erbium luminescence spectrum was observed. The presence of thulium quenches the erbium luminescence, but no direct evidence of energy transfer between Er and Tm was found.

Finally thulium implanted aluminum oxide films were prepared. Time-dependent PL measurements at 650 nm and 790 nm show lifetimes of 0.32±0.05 ms respectively 0.30±0.03 ms. Under 788 nm irradiation, a broad luminescence band in the infrared is observed for samples annealed for 1 hour at 800 °C and 900 °C in vacuum. The lifetime at 1.6 μm is as long as 4 ms. These long lifetimes imply that pure Al_2O_3 may be an excellent host material for an erbium/thulium codoped broadband amplifier.

Contents

1 Introduction

1.1 Communication by optics

All kind of communication (telephone calls, email, video conferencing) is nowadays done by transporting series short pulses of light. The invention of the laser in 1958, that produces intense and coherent light beams, and the development of the fiber as a transparent medium to transmit the light pulses made this happen. Fibers consist of a high refractive core and a surrounding lower refractive index cladding layer. This structure acts as a waveguide: light is confined by internal reflection. The use of fibers allows transmission over long distances.

The growth in the use of optical data transportation systems stimulates the demand for high data transmission rates. In the early times of the fiber communication systems, transmission rates were increased by speeding up the data rate of the bit-streams in the fibers. This speeding up is limited by polarization mode dispersion (pulses spreading out in time), since it becomes more and more difficult to discriminate the pulses. Since the 1990's the capacity has been increased by Wavelength Division Multiplexing (WDM) systems. It combines multiple wavelengths on a slower bit-stream. Today, the data rate of bit-streams of 10-Gb/s is common [1]. 40-Gb/s and terabit (10^{12}) systems are being investigated.

The 'colors' of light that one currently use in telecommunications coincide with the regions where losses caused by Rayleigh scattering and absorption in the fibers is low. These regions are found in the infrared, at 1.5 μm - 1.6 μm (attenuation of 0.15 dB/km) and at 1.3 μm (0.3 dB/km). The local maximum of attenuation at 1.4 μm is caused by vibrational modes of OH^- ions that tend to be present in the fiber. Last year, researchers at Bell Labs reported an elimination of the water absorption in the 1400 nm range, providing a much broader wavelength band than conventional fibers [2].

The spectral range that is used by telecommunication is divided in several parts, the so-called 'bands'. The region from 1530 nm to 1565 nm is called the C-band. In this conventional band the first optical amplifiers were reported, based on erbium doped silicate glasses. The expanding demand for bandwidth caused that other wavelength ranges were explored. Shorter wavelengths are found in the S-band (1450 nm - 1520 nm) and the extended S-band (XS-band, 1270 nm - 1450 nm), longer wavelengths are found in the L-band (1570 nm - 1610 nm) and the extended L-band (XL-band, 1610 nm - 1700 nm). (see for example [3] and [4]).

1.2 Optical amplifiers

To maintain a sufficient light intensity during transportation over long distances, amplification is needed. Since the late 1980's optical amplifiers have been developed. They are mainly based on doping of optically active elements like the rare earth ion erbium. Rare earth ions have a special electronic configuration: the 4f shell electrons are shielded from the surroundings by 5s and 5p electrons. Most transitions between the 4f energy states are parity forbidden, but incorporated in a solid the wave functions of the electrons are disturbed. Mixing of the parity of the states make that radiative transitions become weakly allowed. The lifetime of the luminescence is long: micro or even milliseconds. Higher levels relax rapidly by nonradiative decay (multiphonon emission). Absorption and emission cross sections are relatively small, 10^{-20} - 10^{-21} cm^2. The host surroundings also cause Stark splitting of the energy levels, broadening the spectral shape of the optical transitions [5].

Amplification (stimulated emission) requires population inversion between two states. Erbium doped amplifiers use the transition between the first excited state and the ground state, that luminescence at 1.54 μm. The lifetime is long, in some materials even 20 ms [6]. In principle, population inversion can be reached at relatively low pump powers. However, gain limiting factors like excited state absorption (ESA) and cooperative upconversion (CUC) increase the pump power required to achieve inversion. In erbium doped amplifiers, the erbium is excited at 1480 nm (directly in the first excited state) or at 980 nm (second excited state).

In search for amplification in a wider broadband, one also investigated other rare earth ions.

Thulium doped materials has been investigated for a lasing material around 1.8 μm-2.0 μm [7] and also amplifiers in the S-band (around 1.4 μm) have been reported [8]. These S-band amplifiers make use of the excited state absorption to obtain population inversion between the third and first excited states. The transition occurs at 1.46 μm and requires a more intricate pumping scheme than for erbium. The pumping schemes of thulium doped fibers are based on either one pump source at around 1050 nm (single wavelength pumping) or on two pump sources (dual wavelength pumping). Pump sources of 1200 nm or 1550 nm - 1650 nm in combination with 1050 nm or 1380 nm - 1400 nm are used. Usually, dual wavelength pumping is more efficient.

1.3 Symmorphix

Symmorphix is a company in Sunnyvale, CA, USA. It was founded in October 1998 by a management team from Applied Komatsu Technology (Applied Materials). The main activity is the development of Amplifying Planar Integrated Components (APICs), using proprietary thin-film process technology. APICs represent an advance over traditional fiber amplifiers, like Erbium Doped Fiber Amplifiers (EDFAs) and the more recently developed Raman amplifiers. APICs can be made compact and cost effective, require low pump power and can integrate multiple functions on one chip. They will not replace all conventional amplification technology, but their versatile propeties make them very attractive.

Since January 2001, AMOLF and Symmorphix collaborate on research on materials for optical waveguide amplifiers. In September 2001, I was invited to Symmorphix to present new experimental data on upconversion measurements on erbium/ytterbium doped waveguides, on the effect of anneal treatments of erbium implanted thermal oxide films on silicon and on the new project on thulium. Besides the presentations I assisted the metrology lab in setting up a system to measure upconversion, and in measuring characteristic properties of the waveguides like absorption losses, gain and mode profiles. A tour around the clean room with the deposition, lithography and etching facilities completed the visit.

1.4 What you can find in this report

The research described in this report was performed from January 2001 till March 2002, mainly at the FOM-institute AMOLF in Amsterdam. Several aspects of optical amplifiers were studied: influences of the host material, post anneal treatments, quenching effects. This thesis gives an overview of the research. The optical properties of erbium in Neoceram, a commercially available SiO_2 / Al_2O_3 compound that was considered as a host material, are described in the first part of this thesis. The second chapter concerns a method to incorporate the erbium ions in the host material: ion implantation. The effect of the incoming energy of the ions on the implantation profile (depth and straggle) was studied. The next chapter deals with cooperative upconversion in erbium doped aluminosilicate waveguides. This effect quenches the first excited state and is therefore a gain limiting factor. In chapter four the influence of anneal treatments on the optical properties of erbium is described. The final part is contibuted to thulium and erbium doped silica and aluminumoxide films.

2 Is Neoceram, an Al_2O_3 / SiO_2 compound, a promising material to design waveguide amplifiers?

Neoceram is a commercial Al_2O_3 / SiO_2 compound that is considered as a sputter target for waveguide deposition. In the first section, the elemental composition of a bulk Neoceram sample is described, derived from Rutherford Backscattering Spectrometry (RBS) measurements. In the second part of this chapter, these data are compared to the elemental composition of a deposited film that was made using a similar sputter target. In the next section, photoluminescence (PL) measurements on implanted and unimplanted bulk material are described. Finally, the effect of post implantation anneals on the thin films is described.

2.1 Experimental setup

2.1.1 Rutherford backscattering spectrometry

Rutherford backscattering spectrometry (RBS) measurements were done using a 2 MeV He^+ beam at a scattering angle of 165^o. The incident He^+ ions were directed along the surface normal. A surface barrier detector at an energy resolution of about 13.6 keV was used in combination with a multi channel analyser system to record the energy spectrum of scattered He ions. The RUMP software program was used to analyze the spectra and determine the composition of the material. Energy was calibrated using a Au-coated SiO_2 / Si reference sample.

2.1.2 Photoluminescence spectroscopy

Photoluminescence (PL) measurements were done using a free space setup. The luminescence signal was collected perpendicular to the sample and focused onto the entrance slits of a 96 cm monochromator by a lens with a focus of 10 cm. A liquid nitrogen-cooled germanium detector was used to detect signals in a spectral range between 1.4 μm and 1.7 μm.

To excite the erbium ions, we used two laser lines: the 488 nm line of an argon laser and a 976 nm line of a (tunable) titanium sapphire laser. These lines excite the erbium ions into the $^4F_{7/2}$ and the $^4I_{11/2}$ manifold respectively. To allow for standard lock-in techniques to reduce the noise level, the pump beam had to be modulated on-off. This was done mechanically for the 976 nm beam and by using an acoustic optic modulator (AOM) for the 488 nm beam. Decay traces were recorded at 8 Hz and averaged (256 times) using a digitizing oscilloscope in combination with the Ge detector. The total time response was limited by the detector and was 125 μs.

2.2 Elemental composition of a Neoceram sputter target, measured by Rutherford Backscattering Spectrometry

2.2.1 Sample preparation

A part of a Neoceram bulk sample was implanted at room temperature with 500 keV Er^+ ions to a total dose of 1x10^{15} cm^{-2} and afterwards annealed at 800 ^{o}C for 30 minutes in a vacuum tube furnace. It is difficult to locate the implanted area. The RBS measurement was done outside or at the edge of the implanted area, and hence serve as a measurement of Neoceram composition, but not of the implanted erbium fluence.

2.2.2 Results and discussion

Figure 1 shows the RBS spectrum of bulk Neoceram and a RUMP simulation (drawn line). Since the measurement was done at the edge of the implanted part, a small amount of (implanted) erbium is observed. Therefore, a Gaussian Er profile was taken into account in the simulation, corresponding to an areal density of 0.63x10^{14} cm^{-2}, less than would be expected on the basis of the implantation fluence.

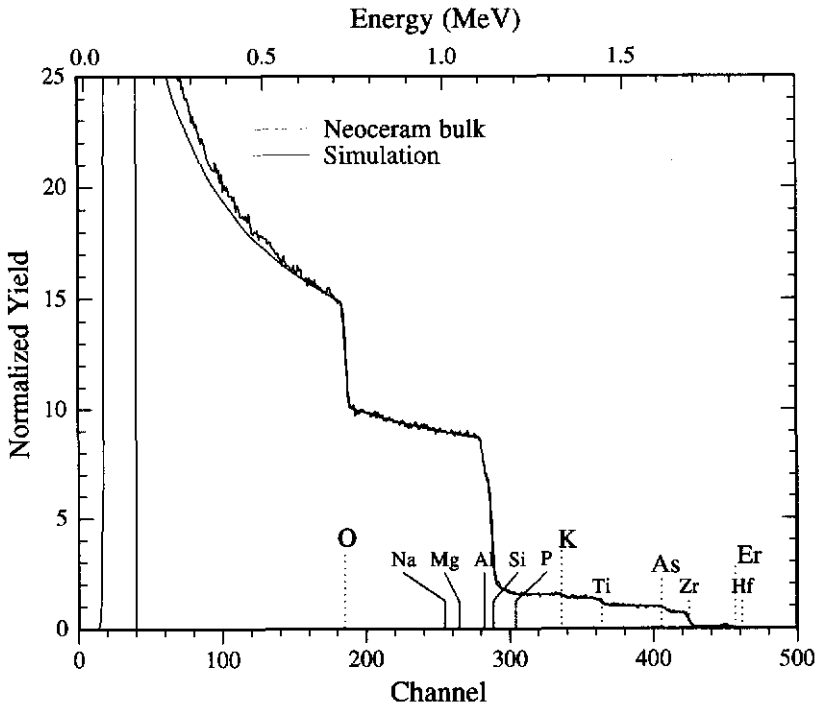

Figure 1: *RBS spectrum of ("unimplanted") Neoceram and a RUMP simulation (drawn line). Indicated are the surface channels of different elements*

A simulation with the RUMP program was performed to determine the elemental composition of bulk Neoceram. The data in table 1 give the best simulation. The standard deviations were determined by the statistical error of the measurement. We have to remark that identification of the heavy elements is uncertain, because the surface channels of these elements are close to each other. For example, the peak attributed to Hf can also be due to Ta or W.

From the data mentioned in table 1, we can make some calculations and estimates. For example, we can make a first order estimate of the relative SiO_2 and Al_2O_3 content in Neoceram. We find a molecular ratio of $Al_2O_3 : SiO_2 = 1{:}5$, ignoring the contribution from oxides of elements with abundance of less than 1%.

We also can calculate the amount of O expected based on the oxide contents of the elements (SiO_2, Al_2O_3, $ZrO_2, TiO_2, K_2O, As_2O_5$). This results in an oxygen fraction of 0.6360, which is, within the error bars, similar to the simulated O fraction of 0.6559.

From the RBS spectrum we also can estimate an upper limit of the amount of Na. In the

Table 1: *Elemental composition of bulk Neoceram results of the simulation.*

Element	*Z*	*Fraction*	$\sigma(\%)$
O	8	0.6559	3.8
Si	14	0.2332	1.9
Al	13	0.0960	7.5
Ti	22	0.0058	14.0
Zr	40	0.0036	4.7
K	19	0.0033	34.0
As	33	0.00213	17.0
Hf	72	0.00007	17.0

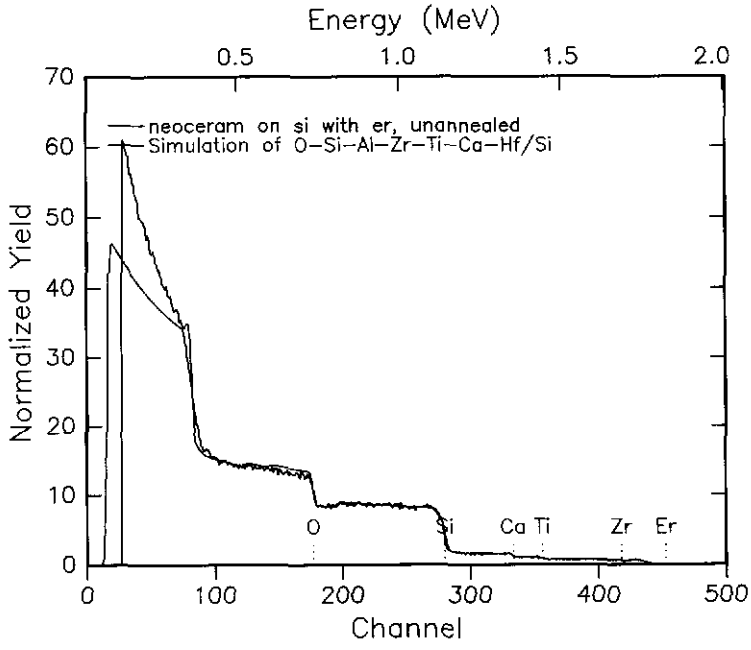

Figure 2: *RBS spectrum of Er implanted Neoceram film on a Si substrate and a RUMP simulation (drawn line). Indicated are the surface channels of different elements.*

spectrum, no Na edge is observed. Taking into account the background signal we estimate the maximum concentration of Na at 3.3×10^{19} atoms/cm^3. This value can be converted to mole fraction using the glass density.

2.2.3 Conclusion

In conclusion, Neoceram consists of Al_2O_3 and SiO_2 in a 1:5 ratio. Small amounts of Zr, Ti, K, As and possibly Hf are also present. The maximum Na concentration is estimated at 3.3×10^{19} atoms/cm^2.

2.3 Composition of unannealed Neoceram waveguide films implanted with 525 keV Er-ions

2.3.1 Sample preparation

A Neoceram film on bare Si was made by plasma vapor deposition. A sample was implanted at 77 K with 525 keV Er^+ ions to a total dose of 1×10^{15} cm^{-2}. After implantation, this sample was not annealed.

2.3.2 Results and discussion

Figure 2 shows the RBS spectrum of the sputtered thin film of Neoceram on silicon. Also a RUMP simulation (drawn line) is shown. Since this measurement was done after an erbium implantation, a Gaussian implantation profile is observed in the spectrum. In the regions of channel number 100-180 and 200-300, some steps are observed. This is due to the change in the concentration of the heavier elements at the substrate/film interface.

Simulations were done to determine the elemental composition of the film. The results are tabulated in table 2. A Gaussian Er profile with an areal density of 1.04×10^{15} cm^{-2} was included. The peak of the Gaussian is (in areal density units) at a depth of 1200×10^{15} cm^{-2} and the full width at half maximum amounts 700×10^{15} cm^{-2}. As mentioned earlier, identification of heavy

Table 2: *Simulated composition of the Neoceram film compared to the composition of the Neoceram bulk sample.*

Element	Z	Bulk Fraction	σ(%)	Film Fraction
O	8	0.66	3.8	0.68
Si	14	0.23	1.9	0.22
Al	13	0.096	7.5	0.082
Ti	22	0.0058	14	0.0064
Zr	40	0.0036	4.7	0.0036
K/Ca	19/20	0.0033	34	-
Ca/Ar	20/21	-	-	0.011
As	33	0.00213	17	-
Hf	72	0.00007	17	0.00004

elements in RBS is uncertain, because the surface channels of these elements are close to each other.

It was wondered if the film would contain indium from solder present in the sputter chamber. Because the indium surface channel (433) incidentally coincides with the peak of the Gaussian erbium distribution in Figure 1, it is not possible to determine the indium profile. If indium is present, its concentration should be smaller than that of erbium.

Comparing the composition of bulk and film Neoceram, shows a different relative amount of the impurities. Especially the amount of Ar/Ca/K in the film is three times higher than in bulk Neoceram. In contrast to bulk Neoceram, no As is observed in the spectrum of the film. The simulation of the film fits better by taking Ca into account instead of K (K was proposed earlier for the bulk target), but it is more likely to contribute this signal to Ar, since this is a common used gas during the deposition of the thin film.

From the data mentioned in table 2, we can make a first order estimate of the relative SiO_2 and Al_2O_3 content in Neoceram film as we did for bulk Neoceram. We find a molecular ratio of Al_2O_3 : $SiO_2 \approx$ 1:5, ignoring the contribution from oxides of elements with abundance of less than 2%. Calculation of the amount of oxygen expected on basis of the oxides of the elements mentioned in Table 2 (SiO_2, Al_2O_3, TiO_2, and CaO), results in an oxygen fraction of 0.59.

2.3.3 Conclusion

The unannealed Neoceram film consists of Al_2O_3 and SiO_2 in a 1:5 ratio, similar to what was found for the bulk target. As in the bulk sample, small amounts of Ca, Zr, Ti and Hf are also present. The argon or calcium density was larger than in the bulk, while no As was found in the film.

2.4 Photoluminescence spectroscopy on bulk Neoceram

A 1.1 mm thick bulk Neoceram sample was partly implanted at room temperature with 500 keV Er^+ ions to a total dose of 1x10^{15} cm^{-2}. Reference samples of Al_2O_3 and SiO_2 films were also implanted to the same dose. After the implantation, all samples were annealed at 800 ^oC for 30 minutes in a vacuum tube furnace.

Figure 3 shows the photoluminescence spectrum of erbium implanted bulk Neoceram. The erbium ions were excited into the $^4F_{11/2}$ manifold, using the 488 nm line of an Argon laser with a pump power of 100 mW. The observed spectrum is broad, the full width at half maximum amounts to approximately 50 nm. Time resolved measurements show that the decay trace at 1.528 μm is single exponential. The lifetime was 5.4 ms. This is lower than that for erbium in the SiO_2 reference samples (10-12 ms), but slightly higher than what was measured for erbium in the Al_2O_3 reference sample (4.5 ms).

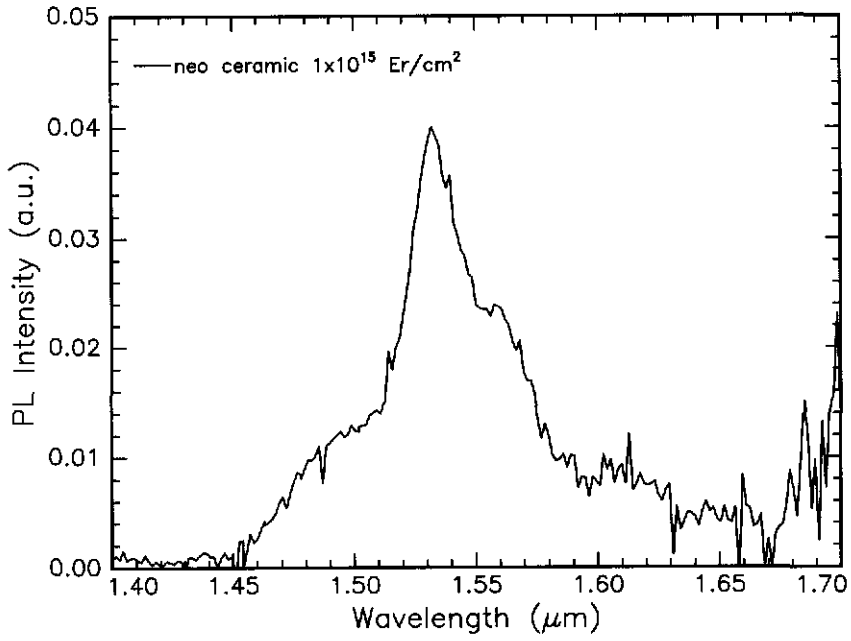

Figure 3: *PL spectrum of Er implanted in bulk Neoceram glass. The sample was annealed for 30 minutes in a vacuum furnace. The erbium ions were excited with the 488 nm line of an argon laser (100 mW).*

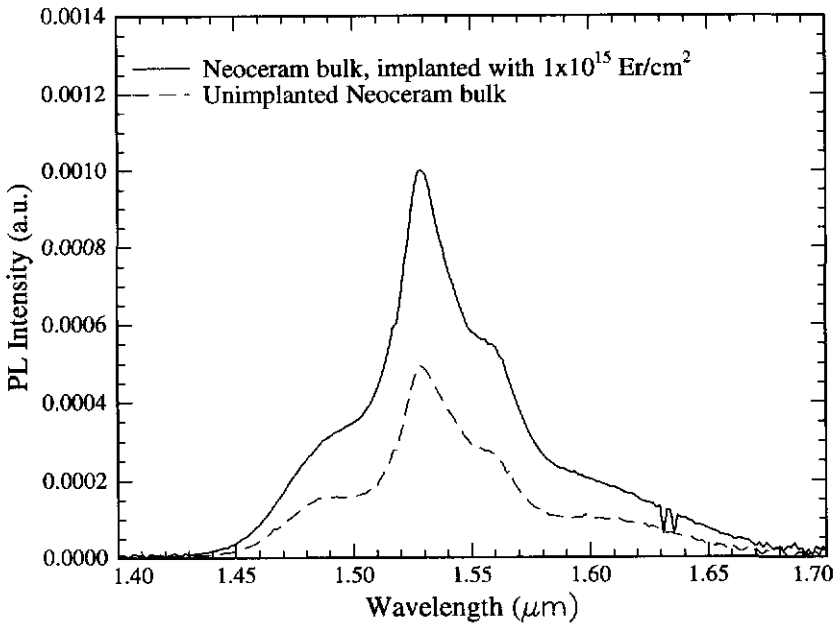

Figure 4: *PL spectrum of Er implanted and unimplanted bulk Neoceram glass, annealed for 30 minutes in a vacuum furnace. The ions were excited with 30 mW pump light at 976 nm.*

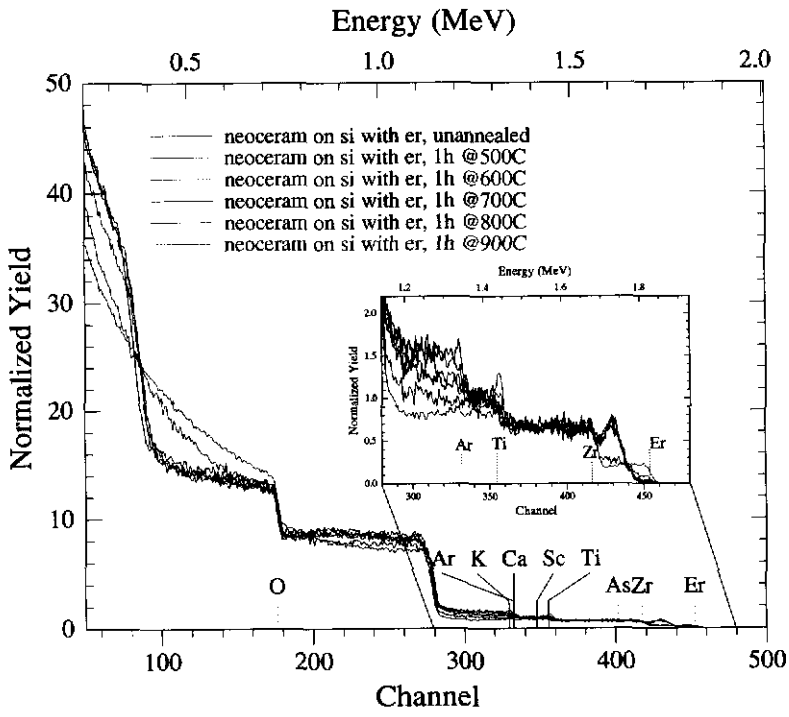

Figure 5: *RBS spectrum of Er implanted Neoceram films for anneal temperatures ranging from 500 to 900° C. The spectrum of the unannealed sample is also shown. The inset shows figure shows a limited spectral range.*

Figure 4 shows the results of photoluminescence measurements in the low pump power regime on unimplanted and erbium implanted bulk Neoceram under 976 nm irradiation (30 mW). We observe two characteristic erbium spectra. The implanted Neoceram shows about twice as much PL intensity as the unimplanted bulk, indicating that the unimplanted bulk neoceram contains a similar dose as the implanted dose ($1x10^{15}$ *ions* cm^{-2}). We can estimate the content of erbium by dividing this value by the thickness of the sample (0.11 cm) and correct for the extra path length due to the incident angle of 30 degrees (and use of Snell's law). Since the volume density of Neoceram is $7.3x10^{22}$ cm^{-3}, we conclude that the unimplanted Neoceram bulk glass contains about 0.12 ppm erbium.

2.5 Annealing Erbium-implanted Neoceram thin films: consequences for structure and optical properties

2.5.1 Sample preparation

Samples cut from a Neoceram film were implanted at 77 K with 525 keV Er^+ *ions to a total dose* of $1x10^{15}$ cm^{-2}. After implantation, the samples were annealed for 60 minutes at 0, 500, 600, 700, 800 or 900 °C in a vacuum tube furnace. The characterization of the unannealed sample was described in 2.3.

2.5.2 Results and discussion

Rutherford Backscattering Spectroscopy

In figure 5 the RBS spectra of erbium implanted Neoceram films are shown with post implantation anneals in vacuum ranging from 0 (unannealed) to 900°C. We observe that the spectra of the two samples with the highest anneal temperatures (800 or 900°C) differ from the others. This is clearly

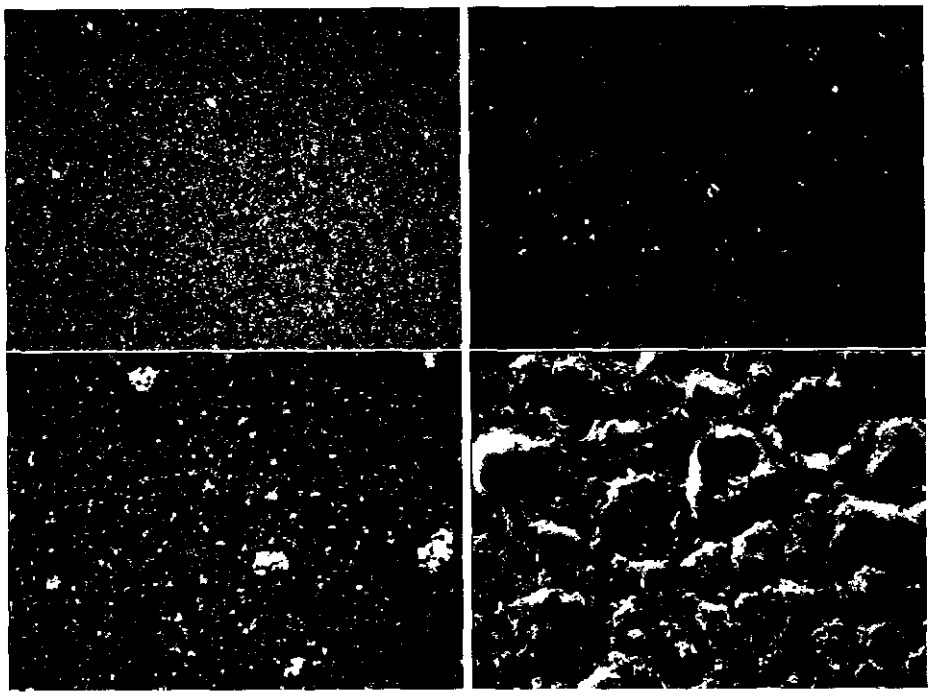

Figure 6: *Images made by optical microscopy of Neoceram thin film samples. The top images show the unannealed sample (left: 200x DF, right: 500x DF), the bottom images show the sample that was annealed for 1h at 900° C in vacuum (left: 200x BF, right: 500x DF).*

seen, especially at the interface of the film with the substrate, around channel 90. Looking at these samples by eye, they appear matt. This suggest a strong change in the morphology of the film.

Furthermore, we observe a drop in the signal around channel 300 when the anneal temperature increases, propably due to out diffusion of Ar. Around the surface channel of Ti (Ch 356) a peak comes up in the spectra of the 800 and 900°C samples. The erbium peak flattens.

Optical Microscopy

Two erbium implanted samples were studied with an optical microscope: the 900°C sample (see figure 6, bottom images) and the unannealed sample as a reference (see figure 6, top images). Two different magnifications were used: 200x and 500x (left and right images in figure 6 respectively). The image of the 900°C sample, magnification 200x, is measured in bright field (BF) conditions; the other images are in dark field (DF) conditions.

The images for the unannealed sample show quite some structure, suggesting large optical inhomogeneities in the Neoceram film. Annealing at 900°C causes a dramatic change in the structure. By changing the depth of focus the height differences in the annealed film were estimated to be up to 4 μm. The observation of large roughness in microscopy is consistent with the changes observed in the RBS spectra.

2.5.3 *Conclusion*

Optical and RBS measurements show that annealing of erbium implanted Neoceram thin film samples at high temperatures causes large inhomogeneities in the film. A similar structure, but much smaller, is also present in the unannealed sample. Due to these inhomogeneities, scattering and losses will be high in Neoceram waveguides. We conclude that Neoceram is not a suitable material for the design of optical amplifiers.

3 Depth profile of erbium ions implanted in Neoceram and SiO_2 waveguide films

Neoceram is a commercial Al_2O_3 / SiO_2 compound that is considered as a sputter target for waveguide deposition. In addition, silica thin films deposited using a double frequency magnetron sputter process are considered. This chapter describes the determination of the depth profile of 525 keV erbium ions implanted in Neoceram and DF SiO_2 measured by Rutherford Backscattering Spectrometry (RBS). The data are compared with TRIM Monte Carlo calculations of ion range. Finally a simple model is derived that can be used to predict Er ion range and straggle for all energies in the range 100 keV – 1 MeV, for both Neoceram and silica.

3.1 Sample description and experimental setup

Samples of Neoceram film on Si and of DF SiO_2 film on Si were implanted at 77 K with 525 keV Er^+ ions to a total dose of $1x10^{15}cm^{-2}$.

Rutherford backscattering spectrometry (RBS) measurements were done using a 2 MeV He^+ beam at a scattering angle of 165°. The incident He^+ ions were directed along the surface normal. A surface barrier detector at an energy resolution of 13.6 keV was used in combination with a multi channel analyzer system to record the energy spectrum of scattered He ions. The RUMP software program was used to analyze the spectra and determine the depth profile of the implanted erbium. Energy was calibrated using a Au-coated SiO_2 / Si reference sample.

TRIM simulations were performed for different erbium implantation energies in SiO_2 in a range of 100 to 800 keV, using the 1998 version of TRIM[1]. In the simulations, a siliconoxide film density of 2.21 g/cm^3 ($6.65x10^{23}$ atoms/cm^3) is used.

3.2 Experiments

3.2.1 RBS spectra and RUMP simulations

Figures 7 and 8 show the RBS spectra of unannealed Neoceram and DF SiO_2 thin films on silicon. The data of the Gaussian erbium profile as used in the RUMP simulations are shown in Table 3. As can be seen in the spectra, a Gaussian erbium profile fits for both. In the spectrum of SiO_2 a signal of argon is observed. For Neoceram, the contribution of erbium is superimposed on that of Hafnium (Hf, surface channel 456) and partially on that of zirconium (Zr, surface channel 418). The contribution of erbium to the signal is shown separately as well. Note that the simulation below channel 100 deviates from the spectrum, especially in the case of DF SiO_2. This is due to uncertainties in the stopping cross sections at low energies. It will cause an extra uncertainty in the determination of the film thickness.

3.2.2 Calculation of the densities of DF SiO_2 and Neoceram

The thicknesses of the films were determined by ellipsometry and amount to 1750 nm for the siliconoxide film and 1380 nm for Neoceram. From the RUMP simulations the areal densities of the films are also known: $1.05x10^{19}$ cm^{-2} for SiO_2 and $1.04x10^{19}$ cm^{-2} for Neoceram, with an estimated standard deviation of 10 %. Combining the optical and RBS data, the volume density (in atoms per cm^3) and the mass density (in g per cm^3) of the films can be calculated. The results are shown in Table 4.

The best fit gives a volume/mass density of DF SiO_2 roughly 10 % lower than for pure silica. Within the error bars it is insignificant. Nevertheless, this may indicate that the DF SiO_2 films are slightly porous. This would be consistent with the fact that, while the composition of the film

[1]See http://www.research.ibm.com/ionbeams/home.htm#SRIM for the latest version of TRIM Monte Carlo simulations.

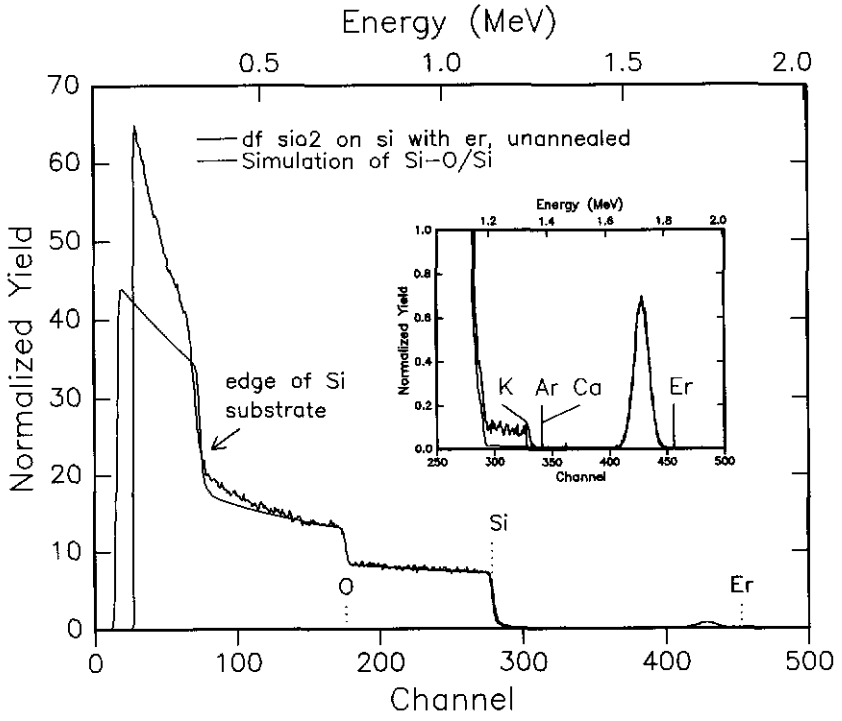

Figure 7: *RBS spectrum of 525 keV erbium implanted in DF SiO_2 film with a RUMP simulation. The inset shows an enlargement of the spectrum in the range from channel 250 to 500.*

Table 3: *Data of the Gaussian erbium profile used in the RUMP simulations.*

	Integral	Depth	FWHM
DF SiO_2	1.05×10^{15} cm^{-2}	1220×10^{15} cm^{-2}	700×10^{15} cm^{-2}
Neoceram	1.04×10^{15} cm^{-2}	1200×10^{15} cm^{-2}	700×10^{15} cm^{-2}

is slightly silicon rich, the index is not higher than that of pure silica. However, such a higher relative amount silicon is not observed in the RBS spectrum.

Table 5 shows the data of Table 3, converted to nanometers using the volume densities of Table 4.

3.2.3 TRIM

TRIM Monte Carlo simulations were performed for erbium in silica with implant energies ranging from 100 to 800 keV, using a mass density of 2.21 g/cm^3 (value for fused silica, equivalent to 6.65×10^{23} atoms/cm^3). Table 6 shows these results. Some values of the parameters used in the simulation are approximate (displacement energy, binding lattice energy). The simulation results are scaled such that the depth and the full width at half maximum of the peak of the erbium profile matches with the values obtained from RBS analysis of Table 5. A corresponding procedure is applied to Neoceram. These results are shown in Table 7.

Figure 9 shows the plots of the raw and corrected data for both the range and straggle as function of the erbium implantation energy of implants in pure silica. For energies between 100 and 900 keV both the ion range and FWHM can be described by linear functions. Table 8 shows the parameters of these linear fits to the corrected TRIM data. The linear fits for pure silica are shown as a lines in Figure 9.

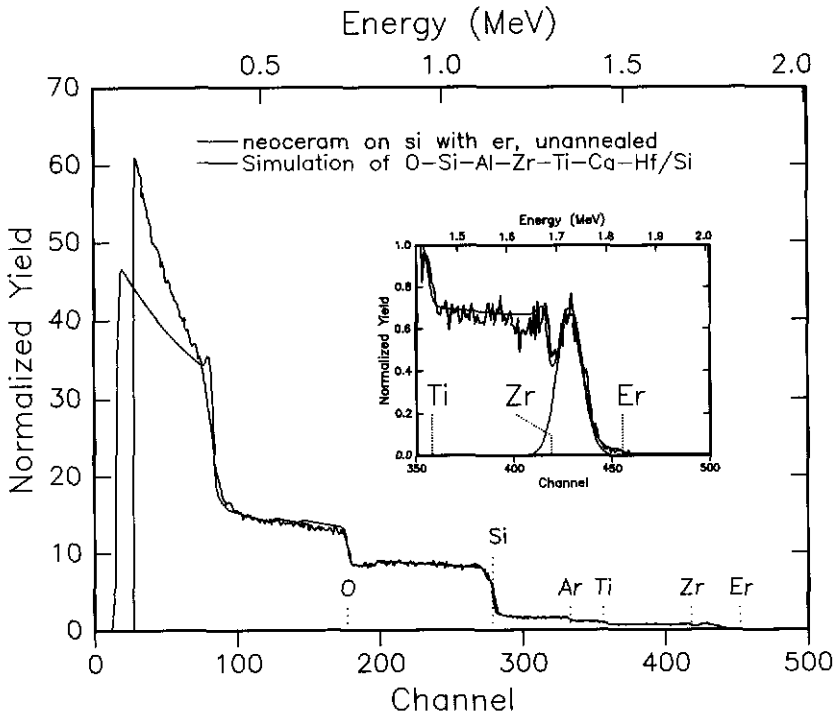

Figure 8: *RBS spectrum of 525 keV erbium implanted Neoceram film with a RUMP simulation. The inset shows the part of the spectrum where the erbium signal is expected. The contribution of erbium to the simulation of Neoceram is shown separately as well.*

Table 4: *Calculation of the volume and mass densities of Neoceram and SiO_2 thin films, using the thickness (from specifications), areal density (from RUMP simulations) and composition of Neoceram (see 2.3).*

	DF SiO_2	Neoceram
Thickness	1750±60 nm	1380±30 nm
Areal density	$1.05\pm0.11\text{x}10^{19}$ cm^{-2}	$1.01\pm0.10\text{x}10^{19}$ cm^{-2}
Volume density	$6.0\pm0.6\text{x}10^{22}$ cm^{-3}	$7.3\pm0.7\text{x}10^{22}$ cm^{-3}
Mass density	1.99±0.21 g cm^{-3}	2.46±0.25 g cm^{-3}

Table 5: *Data of the Gaussian erbium profile of Table 3, expressed in nanometers by dividing the data by the volume densities of Table 4. For DF SiO_2 also the results are calculated assuming the volume density of pure silica, $6.6x10^{22}$ cm^{-3}.*

	Volume density	Depth	FWHM
DF SiO_2	$6.0\text{x}10^{22}$ cm^{-3}	203 nm	117 nm
	$6.6\text{x}10^{22}$ cm^{-3}	185 nm	106 nm
Neoceram	$7.3\text{x}10^{22}$ cm^{-3}	164 nm	96 nm

Table 6: *Data of TRIM 1998 simulations of Er implanted into SiO_2, using a mass density of 2.21 g cm^{-3}. The full width at half maximum is calculated by FWHM = 2 (2 ln 2) $^{0.5}\sigma$.*

Incoming E (keV)	Range (nm)	σ (nm)	FWHM (nm)
100	48	11	26
200	79	17	40
300	108	24	57
400	137	30	71
500	164	36	85
525	**172**	**37**	**87**
600	193	42	99
700	222	47	111
800	251	53	125

Table 7: *Corrected data of TRIM simulations of erbium implanted into SiO_2, DF SiO_2 and Neoceram. Range (R), straggle (σ) and full width at half maximum (F) are given. F is calculated by 2 (2 ln 2) $^{0.5}\sigma$.*

	scaled for pure SiO_2 (2.19 g cm^{-3})			scaled for DF SiO_2 (1.99 g cm^{-3})			scaled for Neoceram (2.46 g cm^{-3})		
Incoming E (keV)	R (nm)	σ (nm)	F (nm)	R (nm)	σ (nm)	F (nm)	R (nm)	σ (nm)	F (nm)
100	52	13	32	57	15	35	46	12	28
200	85	21	49	93	23	54	75	19	44
300	116	30	69	127	32	76	103	26	62
400	147	37	87	162	40	95	131	33	77
500	176	44	104	194	48	114	156	39	92
525	**185**	**45**	**106**	**203**	**50**	**117**	**164**	**40**	**95**
600	208	51	121	228	56	133	184	46	108
700	239	58	135	262	63	149	212	51	121
800	270	65	152	296	71	168	239	58	136

Table 8: *Linear fit ($y = a + b\ x$) through scaled TRIM data of the ion range, straggle and FWHM of erbium in pure silica, DF SiO_2 and Neoceram.*

SiO_2	a (nm)	b (nm/keV)
Range	22.3±0.7	0.310±0.001
Straggle	6.8±0.5	0.073±0.001
FWHM	16.0±1.3	0.172±0.003
DF SiO_2	a (nm)	b (nm/keV)
Range	24.5±0.8	0.340±0.001
Straggle	7.4±0.6	0.081±0.001
FWHM	17.4±1.3	0.190±0.003
Neoceram	a (nm)	b (nm/keV)
Range	19.8±0.7	0.274±0.001
Straggle	6.0±0.5	0.065±0.001
FWHM	14.1±1.1	0.154±0.002

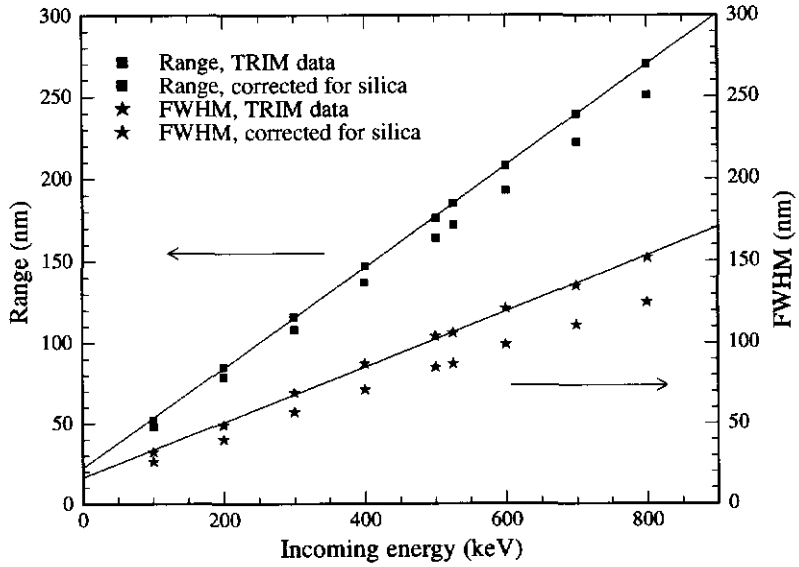

Figure 9: *TRIM and scaled TRIM data of the range (left) and FWHM (right) of erbium ions in pure silica (mass density of 2.19 g cm^{-3}). The lines are linear fits through the corrected data.*

3.3 Conclusions

The volume densities of the DF SiO_2 and Neoceram films are (6.0±0.6) x10^{22} atoms cm^{-3} and (7.3±0.7) x10^{22} atoms cm^{-3}, respectively. The volume and mass densities for DF SiO_2 are 10% below that of pure silica, which, given the error bar, seems not significant. A model is derived that can be used to predict the ion range and straggle of erbium in silica and Neoceram as a function of ion energy.

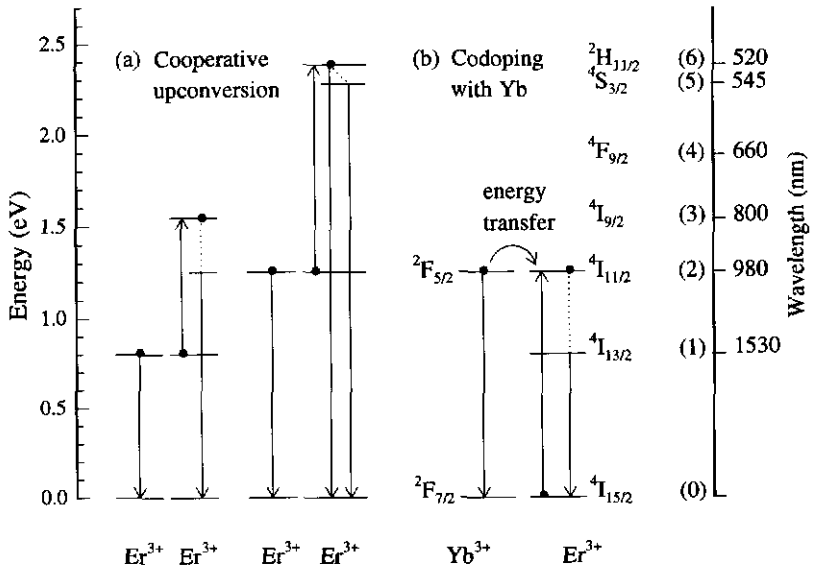

Figure 10: *Er^{3+} energy level diagram showing upconversion processes (a) between two erbium ions giving rise to emission at 980 nm (left) and to emission around 540 nm (right). Figure (b) shows the process of energy transfer from ytterbium to erbium.*

4 Cooperative upconversion in erbium doped systems: a gain limiting factor

4.1 Introduction

Population inversion between two states is required to obtain stimulated emission. In erbium doped amplifiers, concentrations of erbium in the range of 0.1 - 1 at% are required to reach optical gain [9]. Such high contents imply that the distance r between two Er^{3+} ions is small. Electric dipole-dipole interactions ($\sim r^{-6}$) can quench the population in the excited state.

The simplest form of population quenching is energy migration, where an excited ion transfers its energy to an ion in the ground state. This leads to diffusion of the excitation and causes losses if the energy is coupled to a quenching centre like a defect or a hydroxyl group. Another quenching effect is excited state absorption (ESA), where excited ions absorb the pump photons. ESA depends linearly on the pump intensity and the population in the excited state.

Erbium doped systems also show cooperative upconversion (or cross relaxation) processes, where an excited ion transfers its energy to another excited ion. One ion is promoted into a higher manifold, the other is relaxed to the ground state. Figure 10(a) shows two important cross relaxations. In the figure on the left, two erbium ions in the first excited state couple, depleting the first excited level and giving rise to emission at 980 nm. The right one shows two ions in the second excited state. Coupling between these ions populates the manifolds that give rise to emission in the visible (green). Cooperative upconversion depends on the population in the excited states and the coupling efficiency between the two ions.

Some materials are codoped with ytterbium to increase the pump efficiency and to reduce the required pump intensity (and therefore ESA effects). These codoped systems are pumped at 980 nm, since at 980 nm the absorption cross section of Yb^{3+} is about seven times larger than the absorption cross section of Er^{3+}. The ytterbium ions are excited into the $^2F_{5/2}$ level and can transfer their energy to the (resonant) $^4I_{11/2}$ manifold of erbium, see figure 10 (b). For example, the transfer rate in Al_2O_3 amounts to approximately 3.6x10^{-17} cm^3/s for concentrations

of 0.29 at% erbium and 0.28 at% ytterbium [11].

This chapter describes measurements on cooperative upconversion coefficients for two erbium/ytterbium codoped waveguides.

4.2 Experimental

4.2.1 Waveguide specifications

The waveguides of Lot42 and of Lot79a are made of an aluminasilica core embedded in SiO_2 claddings. The core is codoped with erbium and ytterbium. The concentration of erbium is equal to the concentration of ytterbium and amounts to 7.0x10^{20} cm^{-3} in Lot42 and 2.3x10^{20} cm^3 in Lot79a.

On each lot one waveguide was selected for upconversion measurements. The dimensions of the core of the waveguide on Lot42 were 2.5 μm (width) and 0.7 μm (thickness). On Lot79a core of the waveguide was 3.5 μm wide and 1.2 μm thick. During fabrication, the wafers were annealed twice at 800°C for 30 minutes in air.

4.2.2 Experimental setup

To determine the upconversion coefficient of the $^4I_{9/2}$ state (figure 10 (a) right), the Er and Yb ions in the waveguide are pumped with a 1.49 micron diode laser with maximum output power of 45 mW. A tap was used to monitor the power in the input fiber. The power in the control fiber is equal to 5.6% of the power in the input fiber. The luminescence light was collected from the top of the waveguide, using a fiber positioned perpendicular to the waveguide. While varying the pump intensity in the waveguide, the 1530 nm and 976 nm luminescence was monitored, using a liquid nitrogen cooled germanium detector and standard lock-in techniques. Time dependent measurements at 1530 nm were performed at several pump intensities. A band pass filter around 1530 nm was used to filter the luminescence from the laser light.

4.3 Theory

For small pump intensities at 1.49 μm, the Er^{3+} system can be described properly by a four level rate equations model [9]. Remark that at this pump wavelength, the ytterbium is not directly excited. We assume that the Yb does not influence the luminescence of the erbium. This four level rate equations model neglects the population of higher lying levels, e.g. the green luminescence, as well as the amplified spontaneous emission. It is assumed that all population of the second excited state decays non-radiatively to the first excited state (short lifetime, 30 μs in Al_2O_3, < 1 μs in SiO_2).

Under steady state conditions, the population of the first excited state N_1 is given by

$$\begin{aligned} N_1 &= \frac{-b + (b^2 - 4ac)^{0.5}}{2a}, with \\ a &= C_{13}(1 + R_{01}/W_2) \\ b &= W_1 + R_{01} + R_{10} + R_{01}R_{13}/W_2 \\ c &= -NR_{01} \end{aligned} \tag{1}$$

Here the absorption/emission rates R_{ij} are given by $\sigma_{ij} I \,/\, h\nu$, with σ_{ij} the emission/absorption cross sections from the ith to the jth level, I the pump intensity in the waveguide and $h\nu$ the energy of the pump/emission photon. Excited state absorption of the pump (from level 1 to 3) is included by rate R_{13}, cooperative upconversion from the first to the third excited level by C_{13}. N is the total concentration erbium.

Furthermore, under the same conditions the population of the second excited state is

$$N_2 = \frac{C_{13}N_1^2 + R_{13}N_1}{W_2} \tag{2}$$

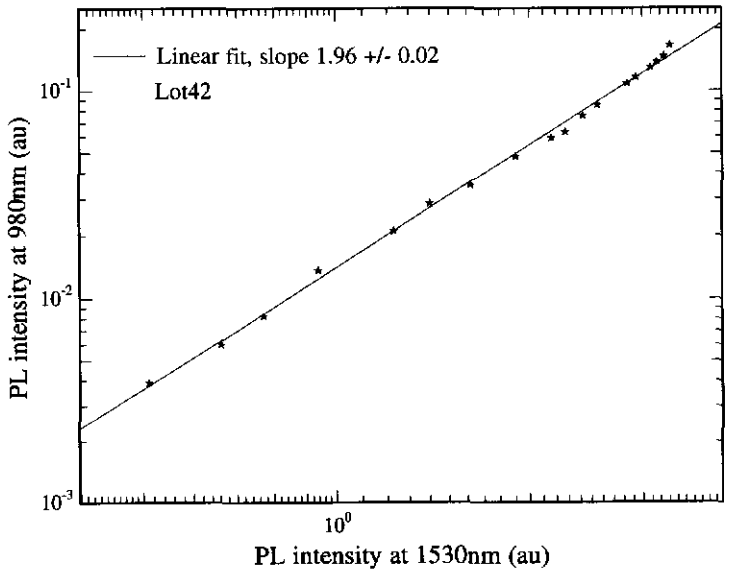

Figure 11: *Photoluminescence intensity at 980 nm versus the photoluminescence at 1530 nm for Lot42.*

From the curves of the photoluminescence at 1530 nm and 980 nm (first en second excited states) versus the pump intensity the upconversion coefficient C_{13} can be determined. Also an estimate of the excited state absorption cross section σ_{13} can be given.

Another way to determine the upconversion coefficient C_{13} is measuring the time evolution of the luminescence of the first excited state. A proper description of this decay can be found by setting the pump rates to zero. The population of N_1 as a function of time after the pump is switched off then becomes:

$$N_1(t) = \frac{N_1(t=0)}{(1 + \frac{N_1(t=0)C_{13}}{W_1})exp(W_1 t) - \frac{N_1(t=0)C_{13}}{W_1}} \tag{3}$$

For normalized decay traces, the only parameters are the decay rate W_1 and the factor $N_1(t = 0)C_{13}$. However, information about the initial excited state population is eliminated. To obtain the upconversion coefficient we have to use the results of the steady state measurements.

Gain simulations can be performed if the populations of the two states are known. Under steady state conditions, the population of the ground state is given by

$$N_0 = \frac{R_{10}N_1 + W_1 N_1 + C_{13}N_1^2}{R_{01}} \tag{4}$$

A formula for the population in the first excited state was already given in equation 1.

4.4 Results and discussion

4.4.1 Lot42: high concentrations of erbium and ytterbium

Figure 11 shows the intensity of 980 nm luminescence versus 1530 nm luminescence on logarithmic scales. Data were obtained by varying the pump power in the pump fiber between 0.7 and 40 mW. From fits at the data in figure 12 (see further on) it is estimated that this corresponds to 0.04 and 4 mW in the waveguide. The data show a linear behavior with a slope of 1.96.

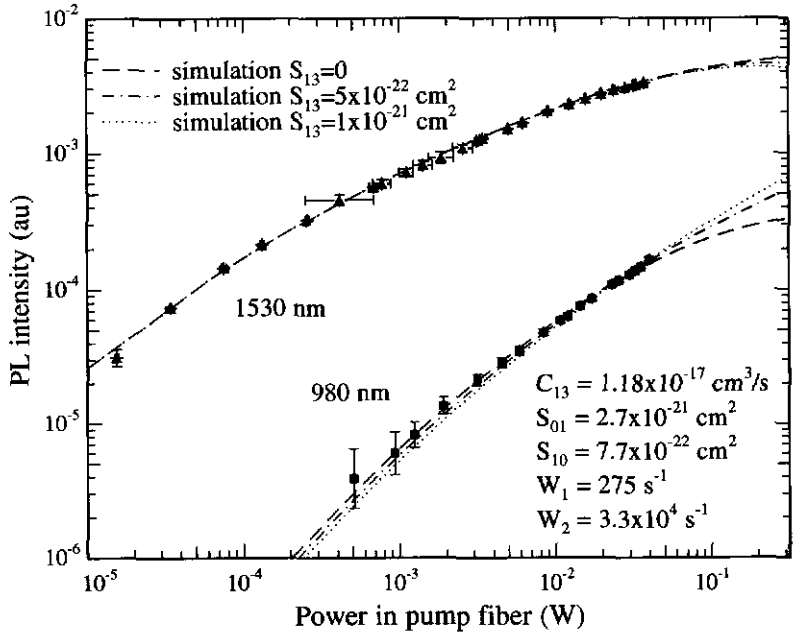

Figure 12: *Photoluminescence intensity data of the 980 nm and 1530 nm levels versus pump intensity, together with fits of formula 1 and 2. Free parameters were the upconversion coefficient, the pump power, and the scale factors for the PL intensities. The excited state absorption cross-section was fixed at σ_{13} =0, 0.5 and 1x10^{-21} cm^3/s.*

In the case only first order cooperative upconversion exists, the data would show a linear behavior with a slope of 2. The fact that the measured slope is slightly less than 2 could be due to second order upconversion (from $^4I_{11/2}$ to $^2H_{11/2}$), because this process depletes the population of the level that emits the 980 nm luminescence.

Steady state PL measurements

Figure 12 shows the photoluminescence intensity data of the 980 nm and 1530 nm signal, together with fits of equation 1 and 2 for three different values of the excited state absorption cross section σ_{13}, namely 0 (no ESA), 0.5 and 1x10^{-21} cm^2.

Equation 1 was fitted through the 1530 nm luminescence data with cooperative upconversion coefficient C_{13}, the collection efficiency and the absolute pump power as free parameters. We assume that the cross-section of the core is 1.75x10^{-8} cm^{-2}. For the pump absorption cross-section σ_{01} and the cross-section for stimulated emission σ_{10} values of erbium in Al_2O_3 were used: 2.7x10^{-21} cm^2 and 0.77x10^{-21} cm^2, respectively [10]. The lifetime was determined to be 3.6 ms, resulting in a decay rate of 275 s^{-1}. After this procedure, equation 2 was used to fit the luminescence data of 980 nm, using the same parameters as for the 1530 nm fit.

In figure 12 the influence of the quenching effects is clearly seen. In all fits, the cooperative upconversion is fixed at 1.18x10^{-17} cm^3/s. If no excited state absorption occurs, the second excited state is populated by the cooperative upconversion process and the curve of the 980 nm photoluminescence equals the square of the 1535 nm PL curve. The influence of excited state absorption will be significant at high pump powers. For curves where ESA is included, we see that the PL at 980 nm increases.

The best fits are obtained for small excited state absorption cross-sections. The upconversion coefficient C_{13} is determined at (1.25±0.3) x10^{-17} cm^3/s and the excited state absorption cross-section σ_{13} is estimated less than 1x10^{-21} cm^2.

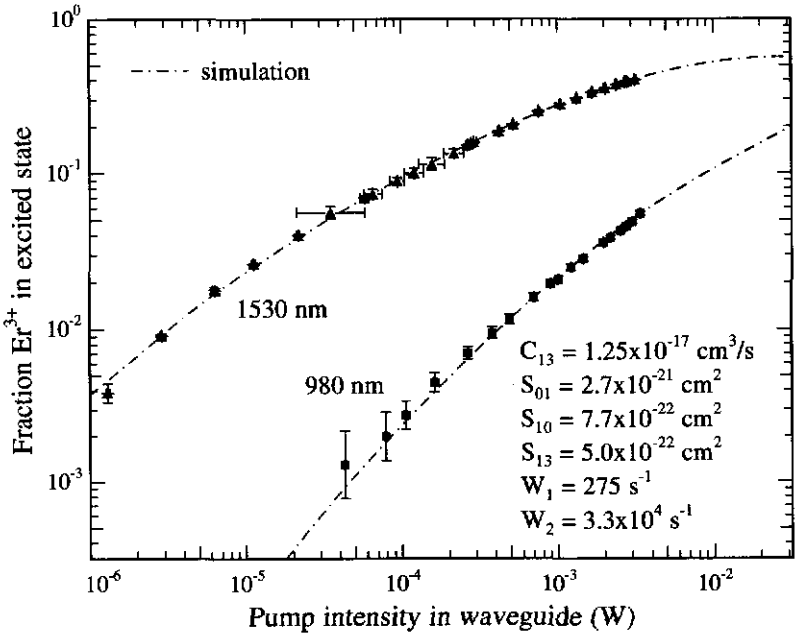

Figure 13: *Population fractions of Er^{3+} in the $^4I_{13/2}$ state (1530 nm) and $^4I_{11/2}$ state (980 nm) versus 1490 nm pump power in the waveguide. Also shown are the fits including effects of upconversion and excited state absorption.*

In the above fits cross-sections σ_{01} and σ_{10} were taken as for erbium in Al_2O_3, while the waveguide cores are made of aluminasilica. Thus we performed new fits for other values of σ_{01} and σ_{10} (fixed). Free parameters during fitting were the upconversion coefficient, the collection efficiency and the absolute pump power. The ESA cross-section was fixed at 5x10^{-22} cm^2. The results are shown in Table 9, where the first row represents the earlier described results. We see that a decrease (increase) of the ratio between the pump absorption and the stimulated emission cross-sections causes an increase (decrease) of the upconversion coefficient C_{13}. This absolute increase (decrease) is comparable to the standard deviation. We conclude that the influence of the values of the cross-sections on the determination of the upconversion coefficient is not significant.

As equations 1 and 2 give the absolute population of Er^{3+} ions in the first and second excited state, the data can be converted to the fraction of Er^{3+} ions in the excited state. The absolute intensity in the waveguide can be obtained by multiplying the intensity in figure 12 by the

Table 9: *Results of the fits of equation 1 and 2 for fixed values of the pump absorption cross-section σ_{01} and the cross-section of the stimulated emission σ_{10}.*

σ_{01} (cm^2)	σ_{10} (cm^2)	σ_{01}/σ_{10}	C_{13} (cm^3/s)
2.70E-21	7.70E-22	3.51	1.25±0.26 x10^{-17}
2.70E-21	3.50E-22	7.71	1.15±0.22 x10^{-17}
2.70E-21	1.44E-21	1.88	1.43±0.26 x10^{-17}
1.35E-21	7.70E-22	1.75	1.51±0.28 x10^{-17}
5.40E-21	7.70E-22	7.01	1.12±0.25 x10^{-17}

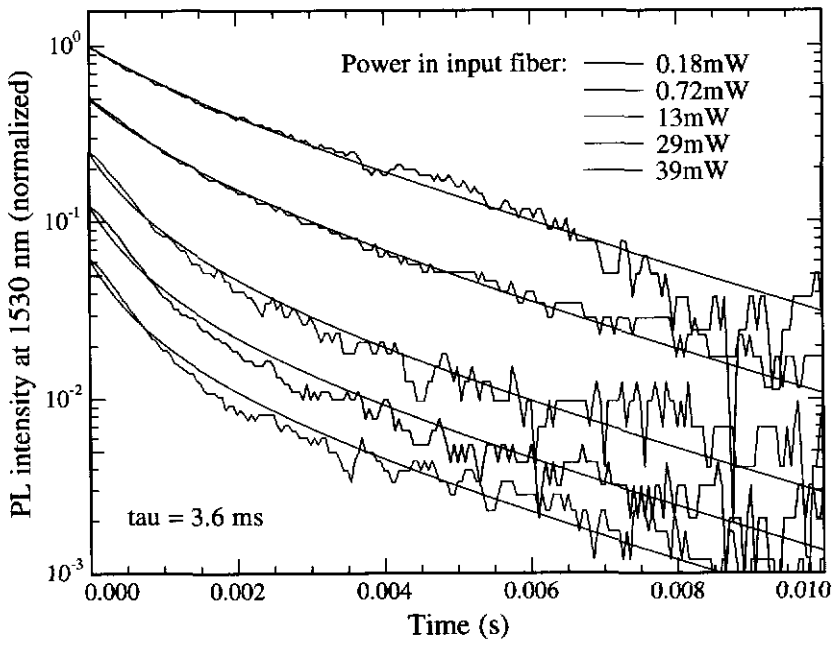

Figure 14: *Decay traces of the $^4I_{13/2}$ state for five pump powers, ranging from 0.18 to 39 mW in the pump fiber. The curves are offset with respect to each other for clarity.*

scale factor of the pump power, determined in the fit procedure. This is done for the fit with σ_{13}=5x10^{-22} cm^2. The result is shown in figure 13. At a pump power of 20 mW in the waveguide (1.1x10^6 W/cm^2), the first excited state will reach a fraction of 0.54; the second excited state a fraction of 0.18.

Time dependent PL measurements

A second method to determine the upconversion mechanism is by measuring the luminescence decay upon switching off the pump light. Decay traces of the $^4I_{13/2}$ state for five pump intensities are shown in figure 14. At low intensities the decay is approximately single exponential. At higher intensities, the initial decay is faster because the upconversion mechanism rapidly reduces the population after switching the pump off. The decay curves can be fit with equation 3. The fits were performed simultaneously, using C_{13} $N_1(t=0)$ and W_1 as free parameters. From the data shown in figure 12 the initial population of the first excited state $N_1(t=0)$ is known and C_{13} can be calculated. The results are shown in Tabel 10. The lifetime of the $^4I_{13/2}$ state was 3.6 ms, resulting in a decay rate of 278 s^{-1}. In figure 14 we see that the simulations fit well for low pump intensities. Therefore, we determine the upconversion coefficient C_{13} at (1.3±0.3) x10^{-17} cm^3/s.

Table 10 shows that under high intensity pumping the decay rate due to the upconversion is larger than 1000 s^{-1}, and thus significantly faster than the spontaneous emission rate of erbium at 1.53 μm.

4.4.2 Lot79a: low concentrations of erbium and ytterbium

The concentration of the erbium and the ytterbium in the waveguides on Lot79a is about three times lower than in the waveguides on Lot42. Measurements on Lot79a show that the luminescence of the second excited state to the ground state (around 980 nm) is very weak. It was hard to fit the data with equations 1 and 2. This indicates that we better can neglect the population of the second excited state. In other words, we assume that the decay of level 2 is very fast ($W_2 \to \infty$).

Table 10: *Summary of the fit results of the decay traces at 1530 nm of Lot42.*

Power in input fiber (mW)	*PL at 1530 nm (au)*	$N_1(t=0)$ *(fraction)*	$N_1(t=0)\ C_{13}$ (s^{-1})	C_{13} $(cm^3 s^{-1})$
0.18	2.6E-4	0.028	294	$1.5\text{x}10^{-17}$
0.72	5.8E-4	0.069	562	$1.2\text{x}10^{-17}$
13	2.2E-3	0.29	1304	$6.4\text{x}10^{-18}$
29	3.0E-3	0.37	1460	$5.6\text{x}10^{-18}$
39	3.3E-3	0.40	1505	$5.4\text{x}10^{-18}$

Table 11: *Summary of the results of the simultaneous fits of the decay traces at 1530 nm of Lot79a.*

Control power (W)	*Input power* (W)	*PL at 1530 nm* (au)	$N_1(t=0)\ C_{13}$ (s^{-1})
6.00E-05	2.14E-03	9.84E-05	340
5.50E-04	1.96E-02	2.42E-04	461
1.10E-03	3.93E-02	2.86E-04	483
1.25E-03	4.46E-02	2.92E-04	548

The equation 1 then becomes

$$\begin{aligned} N_1 &= \frac{-b + (b^2 - 4ac)^{0.5}}{2a}, \ with \\ a &= C_{13} \\ b &= W_1 + R_{01} + R_{10} \\ c &= -NR_{01} \end{aligned} \tag{5}$$

Note that the excited state absorption cross section is eliminated in this equation.

Time dependent PL measurements

Figure 15 shows normalized decay traces taken at four different pump powers in the input fiber (2, 20, 40, 45 mW). Under circumstances without quenching effects like cooperative upconversion, the decay traces are described by a single exponential decay, resulting in a linear plot in figure 15. However, upconversion processes are present and we have to include this quenching effect, equation 3 above. This equation was simultaneously fit to all four curves, also shown in figure 15. From these fits, we obtain a lifetime of 3.5 ms or a decay rate W_1=1/lifetime of 285 s^{-1}.

A summary of all the data needed to calculate the upconversion coefficient C_{13} from these fits is given in Table 11: the values of C_{13} $N_1(t=0)$ obtained from the fits, the four pump powers in the control fiber and in the input fiber, and the PL values measured under steady state conditions at the corresponding pump powers (data taken from figure 16). The PL is directly correlated with the population of the first excited level $N_1(t=0)$. If the scaling factor is known, $N_1(t=0)$ is known and C_{13} can be calculated.

PL measurements under steady state conditions

Steady state measurements with a liquid nitrogen cooled germanium detector were performed twice, resulting in two data sets. The luminescence at 976 nm was also measured using an AgOCs photon multiplier tube (PMT). All data sets are shown in figure 16. It shows the raw PL data versus the pump power in the control fiber. The difference in the two sets of the 1530 nm PL is due to a change in monochromator slit settings and a different coupling between the pump fiber and the waveguide. Also shown in figure 16 is the simultaneously performed fit of equation 5 to the

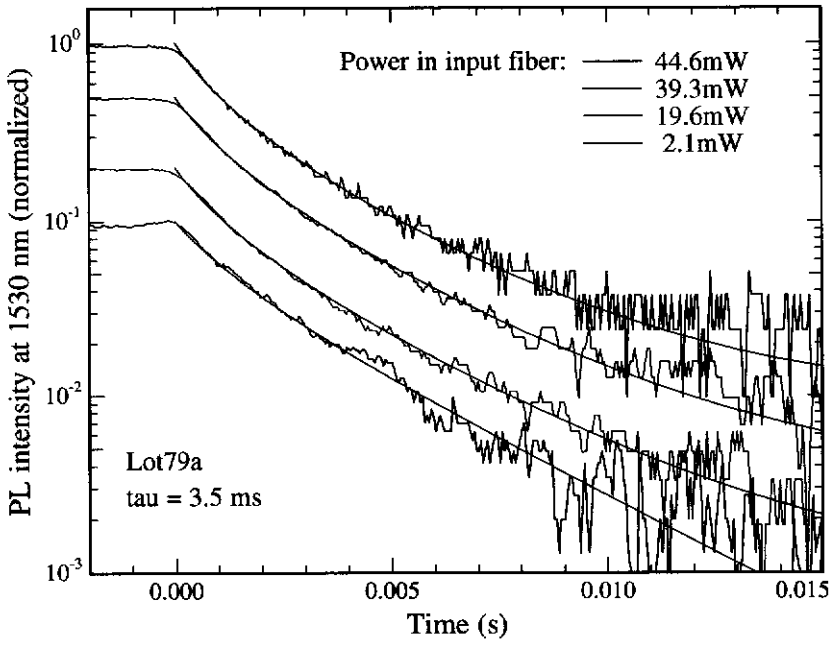

Figure 15: *Decay traces of the luminescence of the first excited level of erbium in Lot79a, at different pump powers and the simultaneously performed fits of equation 3. The curves are offset with respect to each other for clarity.*

two 1530 nm luminescence data sets. Free parameters were the upconversion coefficient C_{13}, the collection efficiency and the intensity. The latter two result in a scale factor of the PL (factor A) and a scale factor of the pump intensity in the waveguide (factor D), respectively. Also fits were performed for C_{13} fixed at values in a range of (3-10)x10^{-18} cm^3/s. From the measurements under steady state conditions it is concluded that the upconversion coefficient C_{13} in this waveguide is equal to (5.5±2) x10^{-18} cm^3/s.

From the fits of equation 5 we obtain a scale factor of the luminescence data at 1530 nm, that we can use to calculate the population in the first excited level under steady state conditions N_1. A pump power of 20 mW in the waveguide (or pump intensity 0.5x10^6 W/cm^{-2}) populates the first excited state with 0.71%. Note that this is about 20 % more than for the waveguide on Lot42 for same pump power. Due to a lower concentration erbium the influence of quenching effects is lower and population inversion can be achieved at lower pump powers.

Since the population of the first excited state is known as a function of the pump power, we also can calculate the values of C_{13} from the decay traces ($N_1(t = 0)$ is known). Table 12 shows the results. For high pump powers the decay rate due to upconversion is about 450 s^{-1}, about twice as large as the sponteneous emission rate of erbium at 1.53 μm. Note that this upconversion rate is lower than the rate we found for Lot42 (> 1000 s^{-1}).

Photoluminescence at 980 nm

For Lot42 we also fitted the photoluminescence at 980 nm, to estimate the excited state absorption cross-section σ_{13}. In the limit that we took for the population in the first excited state N_1, $W_2 \rightarrow \infty$, we should not be able to detect any luminescence at 976 nm. However, we can substitute N_1 in equation 2 by equation 5 and use the in the previous part determined parameters C_{13} and the scale factor for the power to fit equation 2. The only free parameters are then σ_{13} and another scale factor (a scale factor for the PL that includes the lifetime of the second excited state). From these fits, we estimate that σ_{13} is in a range of (2 - 20)x10^{-22} cm^2. One of these fits

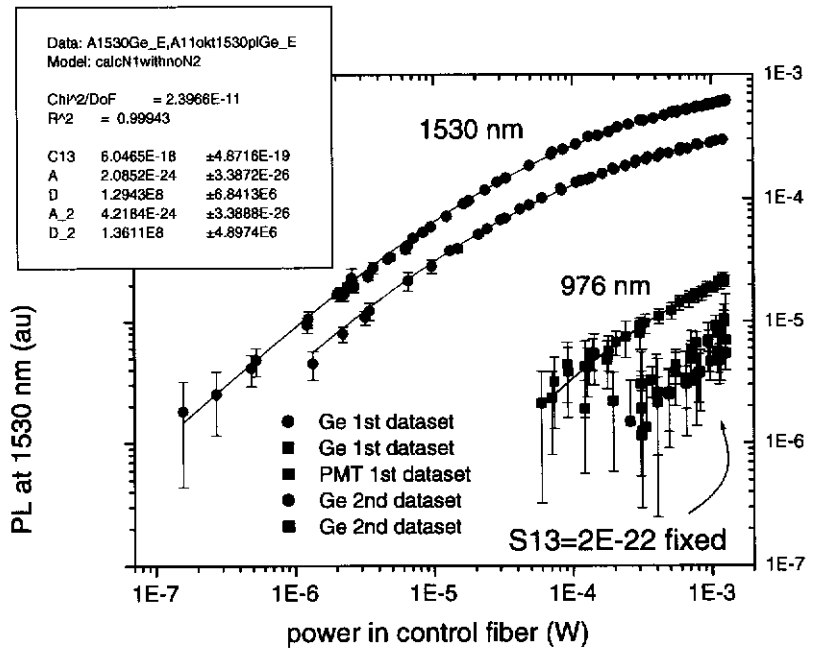

Figure 16: *Measured data, PL intensity versus the power in the control fiber (which is equivalent with 0.028 times the power in the input fiber), together with fits of equation 5 to the 1530 nm luminescence data. The inset shows fit parameters.* C_{13} *is the upconversion coefficient,* A *the scale factor of the 1530 nm PL and* D *the scale factor of the pump power. Also shown is a fit of equation 2 through the 976 nm data with ESA cross section fixed at* $2x10^{-22}$ cm^2*. Using the scale factors* A *en* D*, this figure can be transformed to a (population, intensity in the waveguide) plot.*

is also shown in figure 16 for σ_{13} equal to $2x10^{-22}$ cm^2.

4.5 Conclusions

For two erbium/ytterbium doped waveguides the cooperative upconversion coefficient C_{13} of erbium is determined with steady state and time dependent photoluminescence measurements. For Lot42 with an erbium concentration of $7x10^{20}$ cm^{-3}, C_{13} is determined at (1.3 ± 0.3) $x10^{-17}$ cm^3/s and the excited state absorption cross-section σ_{13} is estimated to be less than $1x10^{-21}$ cm^2. For Lot79a (erbium concentration of $2.3x10^{20}$ cm^{-3}) the upconversion coefficient is lower, (0.55 ± 0.2) $x10^{-17}$ cm^3/s.

Table 12: *Data (see also Table 11) and the calculations of upconversion coefficient* C_{13} *from the decay traces.*

Input power (mW)	*PL at 1530 nm* (au)	$N_1(t=0)$ (cm^{-3})	$N_1(t=0)$ (s^{-1})	$N_1(t=0)$ C_{13} (fraction)	C_{13} (cm^3s^{-1})
2.14	9.84E-05	4.71E19	0.20	340	7.22E-18
19.6	2.42E-04	1.16E20	0.50	461	3.98E-18
39.3	2.86E-04	1.37E20	0.60	483	3.53E-18
44.6	2.92E-04	1.40E20	0.61	548	3.92E-18

5 Optical properties of thulium in silica and aluminum oxide: singly doped and codoped with erbium

5.1 Introduction

The spectroscopic properties of rare earth impurities in glasses have been widely investigated because of their potential applications in science and technology. The growing use of modern communication methods cause that a broad spectral range is used. To compensate for losses over large distances the telecommunication industry is interested in broadband amplifiers in the infrared (where the losses are relatively low). Designs of compact devices where several opto-electronic functions are integrated become essential. Hence waveguide amplifiers combined with multiplexing functions on a single chip have valuable advantages over fiber amplifiers. They also can be processed on a large scale, thus reducing fabrication costs.

Fiber amplifiers have been investigated since the end of the eighties. First, erbium (Er) doped fiber amplifiers have been reported based on the Er^{3+} transition at 1.53 μm. Since a few years, also thulium (Tm) doped fiber amplifiers at 1.4 micron are shown [8]. These S-band amplifiers make use of excited state absorption to obtain population inversion between the third and first excited states. Moreover, it is known that thulium emits light in the wavelength range > 1.7 μm, see for example [12]. It is interesting to combine all these properties in one single system to obtain a broadband amplifier.

For an erbium/thulium co-doped silica-alumina-germanate fiber this was reported in 1999 by Shubochkin *et al.* [13]. The observed luminescence spectra under 980 nm excitation were explained by the existence of a resonant non-radiative energy transfer between erbium and thulium ions. With the pump source wavelength between 945 and 995 nm lasing from erbium ions (around 1.55 μm) and thulium ions (around 1.85-1.96 μm) or from both ions simultaneously was possible depending on parameters of mirrors in the laser cavity, fiber length, pump rate and pump wavelength.

Spectroscopic properties of a erbium/thulium co-doped tellurite system for application in the telecommunications were reported by Shen [14]- [15]. Codoping in glasses was also investigated to enhance upconverted luminescence in the visible and uv, for example by Yeh [16], Zou [17] and Tanabe [18] and coworkers. Furthermore, it has been used to quench the first excited level of erbium to enhance lasing at 2.7 μm [19].

In our research we focus on waveguide materials that can show amplification over a wide wavelength range. We have doped a silica film on silicon and an aluminum oxide film on silica on silicon with thulium by ion implantation. Photoluminescence measurements in the visible and in the infrared wavelength range (steady state and time dependent) were performed at room temperature to investigate the position of the energy levels, relaxation rates and the influence of an post-implantation anneal treatment. The consequences of erbium/thulium co-doping were also studied by luminescence spectroscopy (quenching effects, energy transfer) for silica films. The results are described in this chapter. To the best knowledge of the author, this is the first time that luminescence of thulium in aluminum oxide films has been described.

We have to note that there is some confusion regarding Tm^{3+} energy levels' identifications. We use the notation of Carnall *et al.* for the identification of $^3H_4$ and $^3F_4$ levels (the third and first excited state respectively) [20]. The energy levels of thulium and erbium ions are shown in figure 17.

5.2 Experimental setup

Rutherford Backscattering spectrometry (RBS)

Rutherford backscattering spectrometry measurements were done using a 2 MeV He^+ beam at a scattering angle of 165^o to measure the dose and implantation profile of the implanted ions. The incident He^+ ions were directed along the surface normal. A surface barrier detector at an energy resolution of 13.6 keV was used in combination with a multi channel analyzer system to record the energy spectrum of scattered helium ions. The RUMP software program was used to analyze

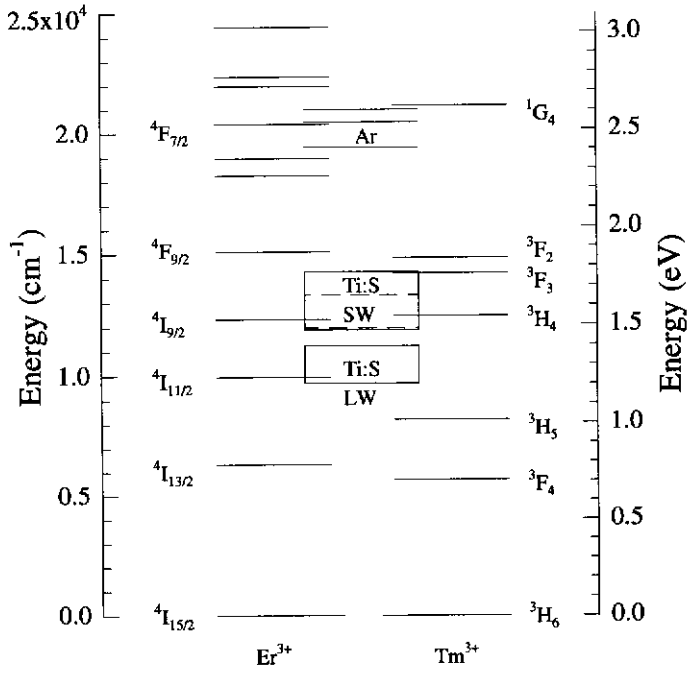

Figure 17: *Energy levels of Er^{3+} and Tm^{3+}. To excite the thulium or the erbium, a suitable laser line has to be chosen. Indicated in green are the laser lines of an argon laser (Ar), in red the lasing range of a tunable titanium sapphire laser (Ti:S). The Ti:S laser can be utilized with short wavelength (SW) or long wavelength optics (LW).*

the spectra and determine depth profile of the implanted erbium. Energy was calibrated using an Au-coated SiO_2 / Si reference sample.

Photoluminescence measurements (PL)
Photoluminescence measurements were done using a free space setup. Mechanically chopped light from a tunable continuous wave titanium sapphire laser irradiated the samples under an incident angle of 30° with the sample normal. The titanium sapphire laser was pumped by a 5 Watt argon laser and was utilized with a short wavelength optics set, enabling laser emission in the range from 700 nm to 840 nm. In some experiments, the argon laser was used to excite the thulium or the erbium. Then, the beam was modulated on and off by an acoustic optic modulator (AOM).

The luminescence signal was collected perpendicular to the sample and focused onto the entrance slits of a 96 cm monochromator by a lens with a focus of 10 cm. Standard lock-in techniques were used to reduce the noise level. A liquid nitrogen-cooled germanium detector was used to detect signals in a spectral range between 900 nm and 1700 nm. The total time response was limited by the Ge detector (125 μs). To collect signals in the wavelength range from 500 nm to 1100 nm a thermoelectrically cooled AgOCs photon multiplier tube (PMT) was used. The total time response of the PMT was about 400 ns.

5.3 Sample characterization

A thermally grown silicon oxide film on a silicon substrate was implanted at room temperature with 900 keV Tm^+ ions to a total dose of about 1x10^{15} cm^{-2}. After implantation the samples were annealed for 1 hour in a vacuum furnace at temperatures of 600, 800 and 900 °C. One sample remained unannealed. Unimplanted samples were annealed at the same temperatures as a reference.

RBS measurements show that the thulium implantation profile is Gaussian with a total areal density of 1.25x10^{15} cm^{-2}. The peak of the profile is at a depth of about 300 nm beneath the surface assuming a density of 6.6x10^{22} atoms cm^{-3}. The full width at half maximum is about 150 nm. The peak concentration is 0.12 at%.

Ellipsometry measurements under three angles of incidence were done to determine the thickness of the SiO_2 layer. Using the optical constants of SiO_2 from Palik (HOC Vol.1, p.759), a perfect fit was obtained resulting in a layer thickness of 9475 $\pm$ 2 nm.

A part of a sputtered Al_2O_3 thin film on top of an approximately 10 μm thick layer of silica on silicon was implanted at room temperature with 900 keV Tm^+ ions to a total dose of 1x10^{15} cm^{-2}. After implantation, the samples were annealed for one hour at different temperatures and in a different ambient: 600°C in vacuum, 800°C in vacuum, 900°C in vacuum and 750°C in air. One sample remained unannealed. As a reference, another part of the same wafer was cut into pieces and annealed.

RBS measurements show that the profile of the implanted thulium is Gaussian and the thickness of the Al_2O_3 film is about 300 nm assuming a density of 1.17x10^{23} cm^{-3}. The total areal density of the implanted thulium is determined at (1.30$\pm$0.08) x10^{15} cm^{-2}. The peak of the profile is at a depth of about 175 nm beneath the surface, the full width at half maximum amounts 94 nm. The peak concentration is 0.11 atomic percent.

Ellipsometry measurements were done under three angles of incidence to determine the thicknesses of the layers. Data for the optical constants were taken from Palik (HOC Vol.1, p.759) for silica and from the Handbook of Thin Film for the aluminum oxide. A perfect fit was obtained with a 9473$\pm$2 nm thick layer of silica and a 349.4$\pm$1.3 nm thick layer of aluminum oxide. Comparing these numbers with the results from RBS, we see that the results for the unimplanted silica film (without Al_2O_3 film) are similar, but for the aluminum oxide film the thickness determined by RBS is smaller. This may indicate that the film is slightly porous.

Erbium and thulium codoped samples were also prepared. A 530 nm thick SiO_2 film on a silicon substrate was implanted with 725 keV Er^+ ions at 77 K to a total dose of 2.5x10^{15} cm^{-2}. Subsequently, the sample was implanted with 725 keV Tm^+ ions at 77 K to doses ranging from 0 to 4x10^{15} cm^{-2}. RBS measurements show that the implantation profiles are nearly Gaussian, with a full width at half maximum of 140 nm. The peak of the profile is found at a depth of 245 nm below the silica-air surface. The concentrations at the maximum of the implantation profile are 0.25 atomic percent for erbium and zero (no thulium implantion), 0.12, 0.28 and 0.56 atomic percent for thulium. Two reference samples containing only thulium with peak concentrations of 0.28 and 0.56 at% were also made. All samples were annealed for 1 hour in a vacuum furnace at 800 °C.

5.4 Photoluminescence on thulium doped silica: results and discussion

5.4.1 Excitation of the thulium

To investigate the optical properties of the thulium (singly) doped samples, we have to choose a suitable wavelength to excite the thulium. Figure 17 shows the energy level diagram of erbium and thulium. It also shows the lines of the argon laser (in green) and the wavelength ranges of the tunable Ti:S laser (in red). Depending on the optics set, laser emission is possible in the short wavelength range (SW) or in the long wavelength range (LW). From this figure, we see that we can excite the thulium using the 476 nm line of the argon laser, which is nearly resonant with the $^1G_4$ level, or the titanium sapphire laser at 790 nm. Then, the thulium ions are excited into the $^3H_4$ manifold.

We investigated the position of this manifold of Tm^{3+} in a singly doped sample with a thulium peak concentration of 0.28 at%. The laser was tuned from 750 nm to 840 nm and the Tm^{3+} transition $^3F_4 \rightarrow {}^3H_6$ (first excited state to ground state) was monitored by detecting the luminescence

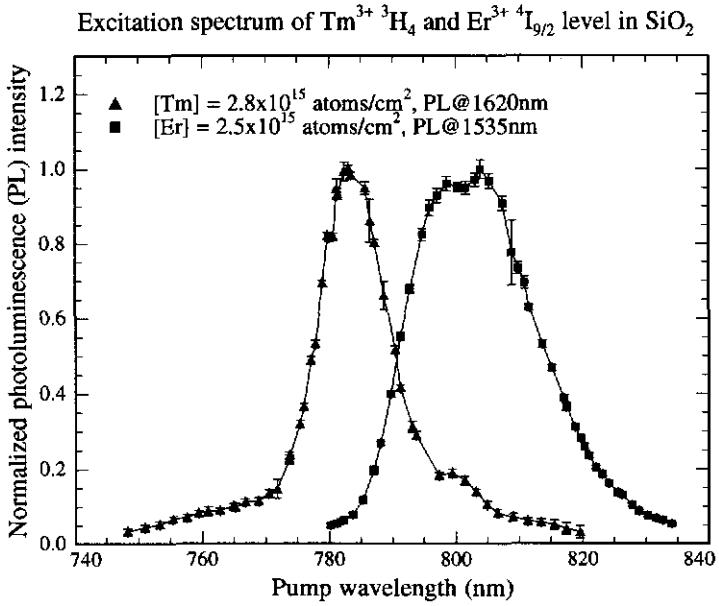

Figure 18: *Normalized photoluminescence at 1620 nm of the $^3F_4$ level of Tm^{3+} in SiO_2 versus pump wavelength. Also shown is the normalized photoluminescence at 1535 nm of the $^4I_{13/2}$ level of Er^{3+} in SiO_2 as a function of pump wavelength.*

at $\lambda = 1620\ nm$[2]. In figure 18 the normalized photoluminescence of this transition versus the excitation wavelength is shown. The thulium spectrum peaks at 783 nm and the full width at half maximum is 14 nm.

Jackson and King reported a similar spectrum by absorption measurements for a thulium-doped silica fiber laser [7]. The peak of the absorption spectrum of the $^3H_4$ level was at 790 nm and the full width at half maximum was about 23 nm. The absorption cross-section at 790 nm was 8.4x10^{-21} cm^2 [7].

5.4.2 The effect of anneals on thulium versus erbium-implanted SiO_2

For erbium in SiO_2 it is known that post implantation anneals increase the photoluminescence intensity and lifetime at 1535 nm [22]. For erbium in hosts with high phonon energies, it is also known that the $^4I_{11/2}$ level has a very fast decay compared to the (millisecond) lifetime of the $^4I_{13/2}$ level. For low pump powers, photoluminescence results can be described properly by a simple two level system. Under steady state conditions, the concentration of excited erbium ions N_1 is given by

$$N_1 = \frac{R_{pump}}{R_{pump} + W_1} N_{total} \tag{6}$$

The pump rate R_{pump} includes the absorption cross-section, the pump intensity and the pump photon energy. W_1 is the total decay rate (radiative and nonradiative) of the first excited state. It is equal to the inverse of the measured lifetime, τ. For low pump powers, the factor reduces to R_{pump}/W_1 (linear regime). Since the photoluminescence intensity is proportional to the radiative decay rate W_1^{rad} times the concentration of the excited ions in the monitored level, the ratio of the PL intensity and the measured lifetime is equal to the total fraction optically active ions.

[2]In literature, the peak of this transition is at 1.7-1.9 μm. However, this is out of range of our germanium detector.

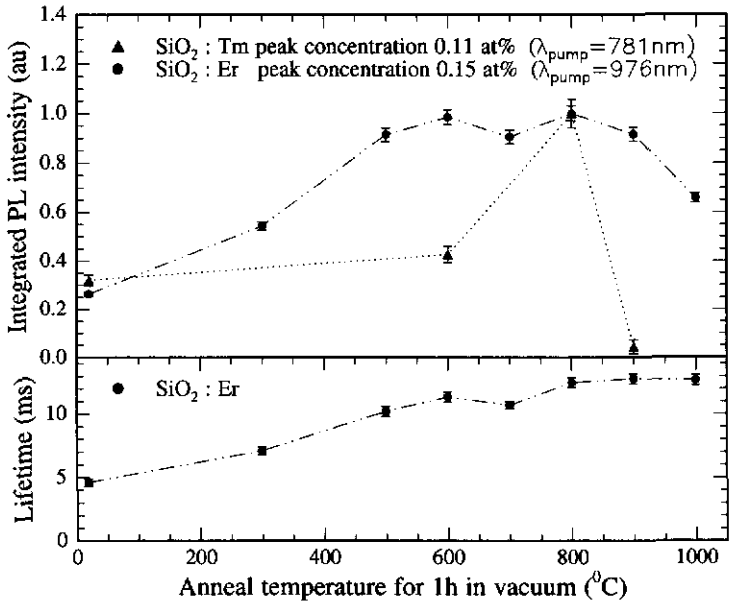

Figure 19: *The top graph shows the normalized integrated PL intensity of Tm^{3+} in SiO_2 versus anneal temperature. The samples were annealed for one hour in a vacuum furnace after implantation. Also shown are the PL intensities at 1535 nm of Er^{3+} in a 10 μm thick thermal oxide film. The bottom graph shows the lifetime of erbium at 1535 nm as a function of anneal temperature.*

We have studied the effect of anneal temperature on the PL intensity and the lifetime of the dopants Tm and Er. Samples that consist of an approximately 10 μm thick (thermally grown) silicon oxide film were used. The peak concentrations are 0.12 at% for the thulium doped samples and 0.15 at% for the erbium doped samples. After implantation samples were annealed for 1 hour in a vacuum furnace, and photoluminescence measurements were done for low pump powers. Using a wavelength of 781 nm, the thulium ions were excited from the ground to the third excited state. PL spectra were measured in the range of 1.4 to 1.7 μm. A broad luminescence band with a maximum at a wavelength larger than the 1.7 μm was observed. This PL was integrated and plotted versus the anneal temperature in figure 19. Similar measurements on the erbium doped SiO_2 samples are also shown (excitation at 976 nm).

For erbium, the lifetime of the unannealed sample was 4.6 ms and increased to 12.6 ms at 800°C. At higher temperatures the PL intensity decreases, while the lifetime remains constant. These observations have been explained by an initially increase of the fraction optically active ions and, at high temperatures, a decrease due to precipitation of erbium [22].

For the thulium doped samples, an increase of the anneal temperature initially causes an increase in PL intensity of the thulium doped samples. A sudden decrease is observed at 900°C. This may be due to the precipitation (like erbium at high temperatures) as well. Based on figure 19, we chose for an 1 hour anneal treatment of 800°C in a vacuum furnace.

5.4.3 Spectra and decay measurements on thulium-doped SiO_2

PL measurements at room temperature were done using the 476 nm line of the argon laser and a photon multiplier tube to collect luminescence in the visible wavelength range. Only the thulium doped silica sample with a thulium peak concentration of 0.11 at% and its unimplanted reference sample (both annealed for one hour anneal at 800°C) were measured. Despite the high pump intensity on the samples of 330 mW, the luminescence due to thulium was weak. A broad luminescence spectrum (due to defects) was observed. Time dependent measurements of the thulium

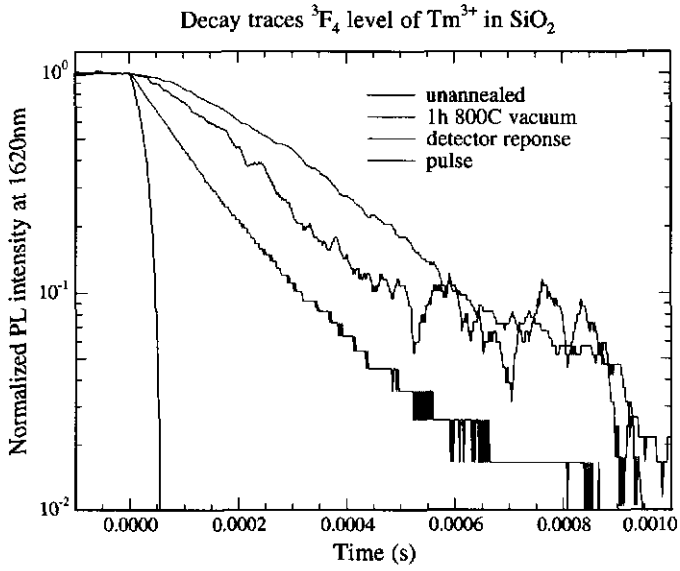

Figure 20: *Decay traces of the $^3F_4$ state of Tm^{3+}, monitored at 1620 nm. Also shown are the detector response and the excitation pulse.*

luminescence at 647 nm and 794 nm result in lifetimes of 0.20±0.02 ms and 0.21±0.03 ms respectively.

Also luminescence in the infrared region was measured at room temperature. As was indicated in 5.4.2, a broad luminescence band with a maximum at a wavelength larger than the 1.7 μm was observed, due to the Tm^{3+} transition $^3F_4 \rightarrow {}^3H_6$. No luminescence of the transition from the third excited state to the first excited state was observed around 1.4 μm. At 1.1 μm a large signal due to defects was found, so that we were not able to resolve thulium luminescence from the second excited state to the ground state. Examples of PL spectra of thulium doped SiO_2 in the wavelength range 1.4 - 1.7 μm can be found in figure 24.

Time dependent measurements at 1620 nm were performed for the thulium doped samples with a peak concentration of 0.28 at%. Figure 20 shows these decay traces for Tm^{3+} in unannealed and annealed SiO_2 films on a logarithmic scale. For comparison, also the laser pulse and the response of the detector are shown. We see that the lifetimes are slightly longer than the detector response (125 μs). This combined to the low signal-to-noise ratio makes it difficult to determine the exact lifetime. As a first order, we estimate the lifetime at 1620 nm to be in the 100-300 μs range. A lifetime of approximately 500 μs was reported by Golding *et al.* for a 1.1 wt % thulium doped silica fiber [21].

S-band amplifiers at 1.4 μm are based on the four-level $^3H_4$ - $^3F_4$ transition. For thulium doped fiber amplifiers it was reported that it is difficult to reach population inversion, since the upper level has a shorter lifetime than the lower level [8]. Note that in our silica films, the upper $^3H_4$ level has a *longer* lifetime than the lower $^3F_4$ level, thus population inversion for S-band amplification at 1.4 μm will be obtained more easily.

5.5 PL measurements on thulium doped Al_2O_3 films

5.5.1 Excitation

In 5.4.1 we discussed the excitation of the thulium ions. Like for SiO_2, we investigated the $^3H_4$ manifold of Tm^{3+} in Al_2O_3 by tuning the titanium-sapphire laser and collect the luminescence of the transition from the first excited state to the ground state at 1.62 μm. Figure 21 shows the results for thulium implanted unannealed and annealed samples (1 hour at 800°C in a vacuum

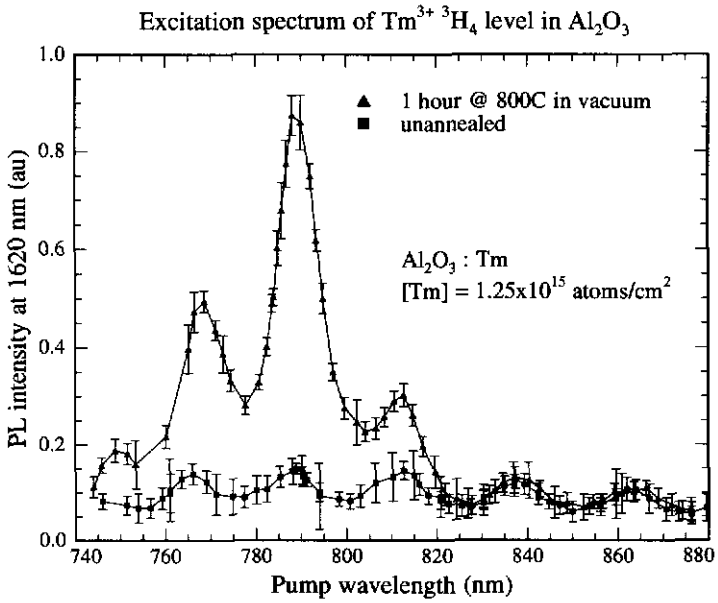

Figure 21: *Excitation spectrum of the $^3H_4$ level of Tm^{3+} in Al_2O_3. The photoluminescence at 1620 nm versus the excitation wavelength is shown for an unannealed sample and the sample that was annealed for one hour at 800° C in vacuum. The oscillations are due to the changing overlap between the pump beam and the implantation profile of the thulium.*

furnace). Calculations show that the observed oscillations are due to variations in the overlap of the pump beam and the thulium implantation profile with changing excitation wavelength. From this graph, we conclude that in order to observe the maximum intensity at 1.62 μm an excitation wavelength of 788 nm has to be used for these samples. However, after deconvolution of the interference effects it will follow that the position of the $^3H_4$ level is at a smaller wavelength, like for thulium in silica (783 nm).

5.5.2 PL spectra, decay traces and the effect of anneals for Tm^{3+} in Al_2O_3

Using an excitation wavelength of 788 nm, PL in the infrared region was measured after the anneal treatment, for all thulium doped Al_2O_3 samples and their unimplanted reference samples. The samples that were annealed for 1 hour at 800 and 900 °C in vacuum show luminescence due to thulium as can be seen in figure 22. The other anneals (600 °C in vacuum and 750 °C in air) and no anneal result in similar luminescence spectra that was observed for the unimplanted reference samples. The ratio of the PL intensity at 1.62 μm of the 800 to 900°C and to the other samples is 1.6 : 1 : 0.32. Time dependent measurements at 1.6 μm show that for the samples were thulium luminescence was observed (800 and 900 °C) the lifetime is 4.0±0.3 ms.

PL spectra in the visible wavelength range were measured for the unimplanted and implanted thulium Al_2O_3 samples that were annealed at 800 °C. The excitation wavelength was 476 nm. The results are shown in Figure 23. A broad luminescence band around 600 nm is observed for both samples. The thulium doped sample also shows peaks around 650 and 790 nm. The superimposed oscillations are due to the interference effect of the luminescence in the Al_2O_3 / SiO_2 films. Time dependent measurements under the same conditions show lifetimes of 0.32±0.05 ms at 647 nm and 0.30±0.03 ms at 790 nm.

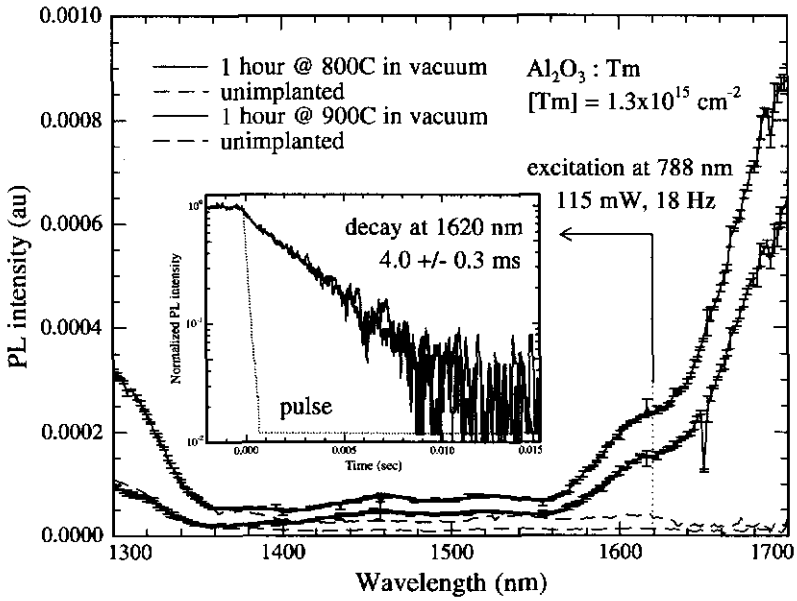

Figure 22: *Photoluminescence spectra from 1.3 μm to 1.7 μm of thulium doped Al_2O_3 thin films and unimplanted reference samples. The samples have been annealed for one hour in vacuum at 800° C and 900° C. The inset shows the decay traces at 1.62 μm.*

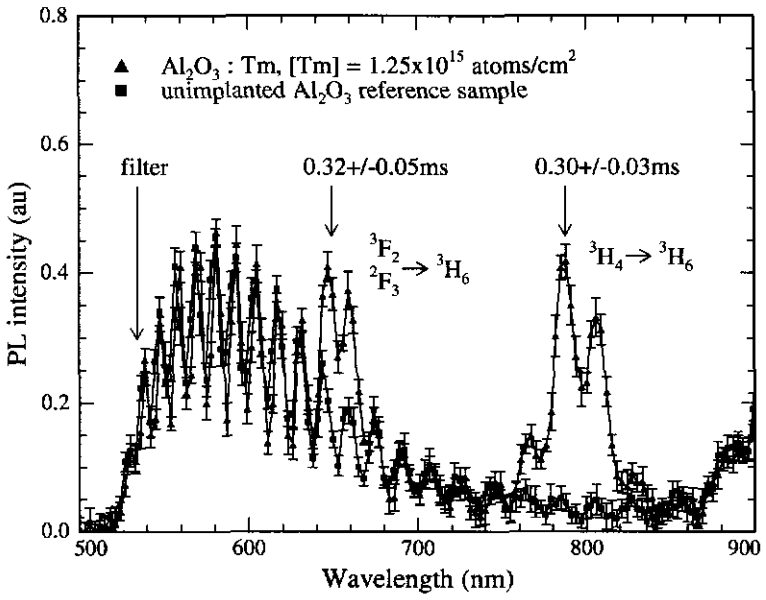

Figure 23: *PL spectrum of thulium implanted Al_2O_3 film and an unimplanted reference sample. Both samples were annealed for 1 hour in a vacuum furnace at 800 °C. The 476 nm line of the Argon laser was used to excite the thulium ions. The luminescence of the thulium at 650 nm and 800 nm is weak.*

5.6 PL measurements on erbium and thulium codoped silica

5.6.1 Excitation

We like to focus on energy transfer effects between the first excited state of Er^{3+} ($^4I_{13/2}$) and the first excited state of Tm^{3+} ($^3F_4$). In order to excite one of the two species, we have to choose the excitation wavelength very carefully. From figure 17 we see that we can use the argon laser to excite the erbium in the $^4F_{7/2}$ manifold at 488 nm and the $^2H_{11/2}$ at 515 nm. Or we can use the titanium sapphire laser to excite the $^4I_{9/2}$ manifold at 800 nm and the $4I_{11/2}$ manifold at 980 nm. We preferred to excite the erbium into one of the lower energy states, thus reducing the possibility of energy transfer at higher energy states.

First, we investigated the position of the $^4I_{9/2}$ manifold of Er^{3+}. A singly doped sample with an erbium peak concentration of 0.25 at% was used. While tuning the titanium sapphire laser, the photoluminescence signal at 1535 nm, due to the Er^{3+} transition $^4I_{13/2} \rightarrow ^4 I_{15/2}$ (first excited state $\rightarrow$ ground state), was monitored. The data are shown in figure 18. In this figure also the thulium excitation spectrum of the $^3H_4$ manifold was shown. The erbium spectrum is broad (FWHM of 25 nm) and peaks at 802 nm. Like we expected from the energy level diagram, we see that the erbium spectrum partly overlaps with the thulium spectrum. To excite the erbium but not the thulium the excitation wavelength has to be larger than 820 nm.

The data in figure 18 have been normalized. In absolute numbers, the peak of the erbium excitation spectrum is about 2.25 times higher than the peak of the thulium excitation spectrum, after corrections for the pump power and the spectral response of the germanium detector. The areal density of erbium in the film was about 10 % lower than the areal density of thulium.

5.6.2 PL spectra and decay measurements

PL spectra of the codoped samples were measured using pump wavelength at 800 nm and at 820 nm. At 820 nm irradiation, the erbium is not pumped efficiently. It turns out that excitation at 800 nm gives similar results as excitation at 820 nm. This is not in contradiction with the results in figure 18, since the ratio of the erbium PL at 1535 nm to the thulium PL at 1620 nm appeared to be approximately the same in both cases.

PL spectra from 1.4 μm to 1.7 μm and decay traces at 1535 nm are shown in figure 24, using excitation at 800 nm (left) and 515 nm (right). Codoped as well as singly doped samples were measured. All data are corrected for the spectral response of the detector. The two top graphs show the raw spectra. It is clearly observed that an increase of the concentration of thulium causes a decrease in PL intensity at 1535 nm (peak of a typical erbium spectrum). Excitation at 800 nm also shows an increase of the PL intensity in the wavelength range from 1600 to 1700 nm as the thulium concentration is increased.

The middle graphs show the same data, but normalized at 1535 nm. The graph on the left clearly shows that the increase of PL intensity at large wavelengths is due to (direct) excitation of the thulium. The difference between the spectra of the singly doped thulium sample and the erbium/thulium-codoped sample is small. The right graph shows that at 515 nm no thulium ions are excited. On this relative scale, the PL intensity at 1700 nm increases slightly with increasing thulium concentration. From these data, it is hard to say whether this is due to the normalization at 1535 nm or to energy transfer from erbium to thulium.

The bottom graphs show the decay traces of the PL intensity at 1535 nm on a logarithmic scale for samples with thulium peak concentrations of 0, 0.12, 0.28 and 0.56 at%. The singly doped erbium sample show a single exponential decay with a lifetime of 11.3±0.2 ms. Upon addition of thulium the decay becomes nonsingle exponential.

Under 800 nm excitation the decay at 1535 nm becomes faster as the thulium concentration increases (left graph). This can be explained by the fast decay of the thulium, since in the spectra of the thulium singly doped samples some luminescence at 1535 nm is observed. The decay of this signal causes the initially fast decay.

Under excitation at 515 nm however, the decay traces at 1535 nm are independent of the concentration of thulium (right graph). At this stage, these data remain unexplained.

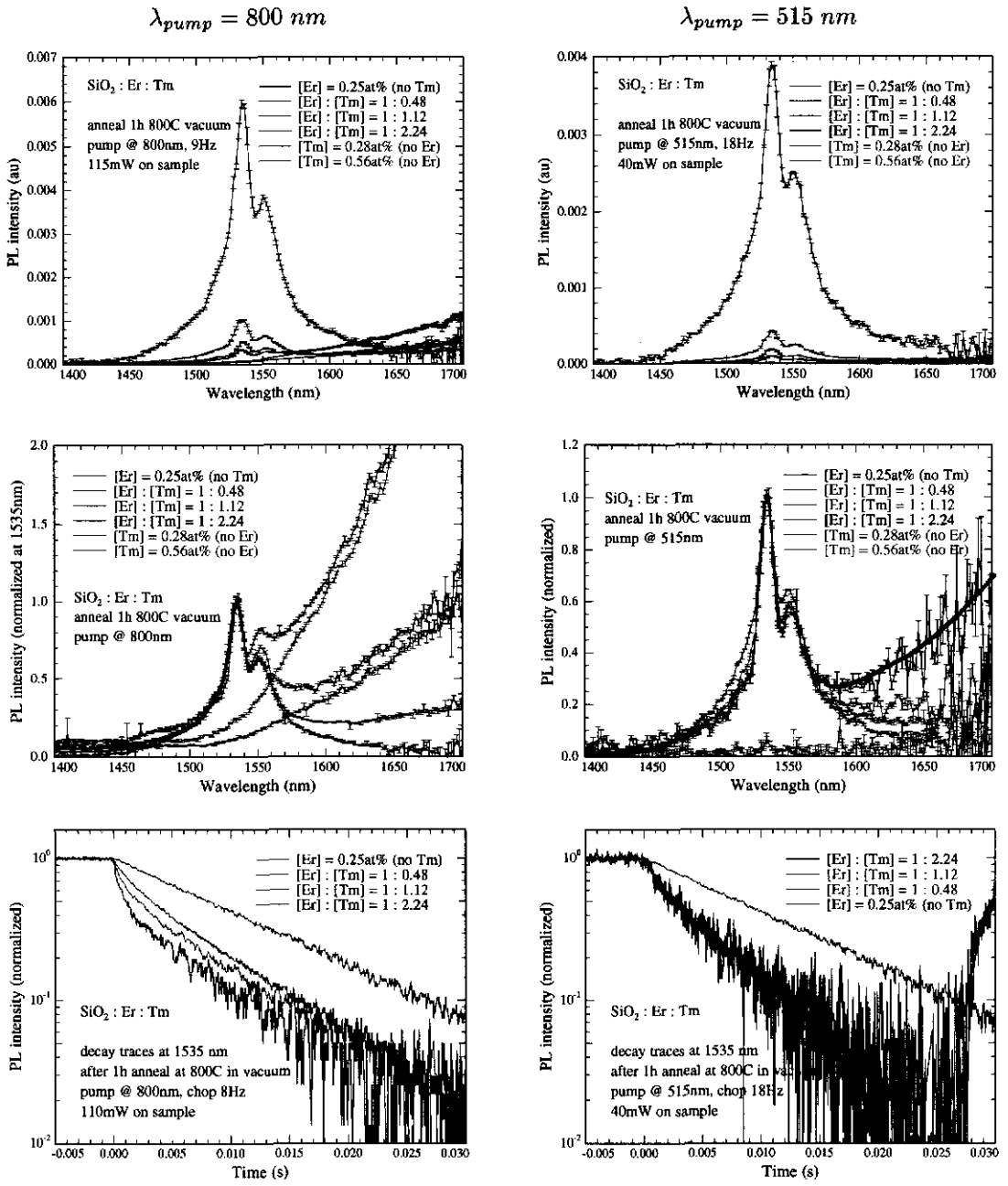

Figure 24: *PL spectra and lifetimes at 1535 nm of erbium and thulium codoped samples. Excitation wavelengths are 800 nm (left) and 515 nm (right).*

5.7 Conclusions

We have investigated the optical properties of thulium implanted silica and aluminum oxide films. Samples that have been annealed for one hour at 800 °C in vacuum show room temperature photoluminescence. Luminescence at 1.6 μm (due to the transition between the first excited state and the ground state) shows a fast decay for the silica samples (100-300 μs). For thulium in aluminum oxide lifetimes of 4.0 ms were found. Under 476 nm excitation we were able to measure the decay of the $^3H_4$ (790 nm) and the $^3F_{2,3}$ (650 nm) states. For thulium in silica, these luminescence lifetimes were determined at 0.21±0.03 ms and 0.20±0.02 ms at 794 nm and 650 nm respectively and 0.30±0.03 ms and 0.32±0.05 ms for thulium in aluminum oxide. Furthermore, we have found that for singly doped silica films, the excitation spectrum of the $^3H_4$ manifold of Tm^{3+} shows a maximum around 783 nm and a full width at half maximum of 14 nm, where the Er^{3+} $^4I_{9/2}$ has a maximum at 802 nm and a FWHM of 25 nm. Photoluminescence measurements on codoped silica samples show quenching of the erbium luminescence at 1.53 μm by the presence of thulium. No direct evidence is found for energy transfer from Er^{3+} $^4I_{13/2}$ to Tm^{3+} $^3F_4$. The long lifetimes in Al_2O_3 imply that this material may be an excellent host material for an erbium/thulium doped broadband amplifier.

References

[1] *Fiber Optics Tunes Up*, IEEE Spectrum, February 2002, p. 9

[2] W.H. Knox, The *future of WDM*, OPN Trends, vol 1, no 1, March 2001, Optical Society of America, p.4-6

[3] B. Cole, M.L. Dennis, *S-band amplification in a thulium doped silicate fiber*, OFC 2001, Technical Digest Postconference Edition vol. 2, p. TuQ3-1-3, Opt. Soc. America, Washington DC, USA, 2001

[4] S. Bigo, *Where is the fun in designing 10 Tbit/s transmission systems?*, ECOC 2001, Amsterdam, the Netherlands, 2001, vol. 5, tutorial Mo.M.2.1, p. 2-24

[5] S. Hüffner, *Optical Spectra of Transparant Rare-Earth Compounds*, Academic, New York, 1978

[6] E. Snoeks, *Optical doping of silica by erbium ion implantation*, PhD thesis, University Utrecht, 1995

[7] S.D. Jackson and T.A. King, *High-power diode-cladding-pumped Tm-doped silica fiber laser* Optics Letters **23** 18 (1998) 1462-1464

[8] T. Sakamoto, *S-band fiber optic amplifiers* Optical Fiber Conference 2001, TuQ1-2

[9] G.N. van der Hoven et al, *Upconversion in Er-implantated Al_2O_3 waveguides*, Journal of Applied Physics, vol 79 no 3, p 1258-66, 1996

[10] G.N. van der Hoven, J.A. van der Elsken, A. Polman, C. van Dam, K.W.M. van Uffelen, M.K. Smit, *Absorption and emission cross sections of Er^{3+} in Al_2O_3 waveguides*, Applied Optics, vol 36 no 15, p 3338-41, 1997

[11] C. Strohhöfer, A. Polman, *Absorption and emission spectroscopy in Er^{3+} - Yb^{+3} doped aluminum oxide waveguides*, submitted to Optical Materials

[12] D.C. Hanna, I.M. Jauncey, R.M. Percival, I.R. Perry, R.G. Smart, P.J. Suni, J.E. Townsend, and A.C. Tropper, *Continuous-wave oscillation of a monomode thulium-doped fibre laser* Electronics Letters **24** 19 (1988), 1222-3

[13] R.L. Shubochkin, V.A. Kozlov, S.R. Han, T.F. Morse and K. Oh, *Er^{3+}/Tm^{3+} co-doped silica fiber laser* Advanced Solid-State Lasers. OSA Trend in Optics and Photonics Series Vol.26. Opt. Soc. America, Washington, DC, USA; 1999; xvi+755 pp. p.167-71.

[14] S. Shen, M. Naftaly and A. Jha, *Tm^{3+} and Er^{3+}-doped tellurite glass fibers for a broadband amplifier at 1430 to 1600 nm* Proceedings of the SPIE vol 3849 (1999), 103-110

[15] S. Shen, M. Naftaly, A. Jha, and S.J. Wilson, *Thulium-doped tellurite glasses for S-band amplification* Optical Fiber Conference 2001 TuQ6-1

[16] D. C. Yeh, R.R. Petrin, W.A. Sibley, V. Madigou, J.L. Adam and M.J. Suscavage, *Energy transfer between Er^{3+} and Tm^{3+} ions in a barium fluoride-thorium fluoride glass* Physical Review B **39** 1 (1989), 80-90

[17] X. Zou, A. Shikida, H. Yanagita, and H. Toratani, *Mechanisms of upconverion fluorescences in Er^{3+}, Tm^{3+} codoped fluorozircoaluminate glasses* Journal of Non-Crystalline Solids **181** (1995), 100-109

[18] S. Tanabe, K. Suzuki, N. Soga, and T. Hanada, *Mechanisms and concentration dependence of Tm^{3+} blue and Er^{3+} green up-conversio in codoped glasses by red-laser pumping* Journal of Luminescence **65** (1995), 247-255

[19] Y.G. Choi, K.H. Kim, B.J. Lee, Y.B. Shin, Y.S. Kim, and J. Heo, *Emission properties of the Er^{3+}: ${}^4I_{11/2} \rightarrow {}^4I_{13/2}$ transition in Er^{3+}- and Er^{3+}/Tm^{3+}-doped Ge-Ga-As-S glasses*, Journal of Non-Crystalline Solids **278** (2000), 137-144

[20] W.T. Carnall, P.R. Fields, and K. Rajnak, *Electronic energy levels in the trivalent lanthanide aquo ions. I. Pr^{3+}, Nd^{3+}, Pm^{3+}, Sm^{3+}, Dy^{3+}, Ho^{3+}, Er^{3+}, and Tm^{3+}* Journal of Chemical Physics, **49** 10 (1968), 4424-4442

[21] P.S. Golding, S.D. Jackson, P.-K. Tsai, B.C. Dickinson, and T.A. King, *Efficient high power operation of a Tm-doped silica fiber laser pumped at 1.319 μm* Optics Communications **175** (2000) 179-183

[22] A. Polman, D.C. Jacobson, D.J. Eaglesham, and J.M. Poate, *Optical doping of waveguide materials by MeV Er implantation* Journal of Applied Physics **70** 1 (1991), 3778-3784